

Fluoroalkylated Silicon-Containing Surfaces – Estimation of Solid Surface Energy

Shreerang S. Chhatre,[†] Jesus O. Guardado,^{} Brian M. Moore,[§] Timothy S. Haddad,[¥] Joseph M. Mabry,
[§] Gareth H. McKinley,^{‡*} and Robert E. Cohen^{†*}*

[[†]] Prof. Robert E. Cohen, and Shreerang S. Chhatre, Department of Chemical Engineering,
Massachusetts Institute of Technology, Cambridge, Massachusetts 02139

E-mail: recohen@mit.edu

[^{*}] Jesus O. Guardado, Department of Materials Science and Engineering, Massachusetts Institute of
Technology, Cambridge, Massachusetts 02139

[[‡]] Prof. Gareth H. McKinley, Department of Mechanical Engineering, Massachusetts Institute of
Technology, Cambridge, Massachusetts 02139

E-mail: gareth@mit.edu

[[§]] Dr. Joseph M. Mabry, and Mr. Brian M. Moore, Space and Missile Propulsion Division, Air Force
Research Laboratory, Edwards Air Force Base, California 93524

[[¥]] Dr. Timothy S. Haddad, ERC Incorporated, Air Force Research Laboratory, Edwards Air Force
Base, California 93524

**RECEIVED DATE (to be automatically inserted after your manuscript is accepted if required
according to the journal that you are submitting your paper to)**

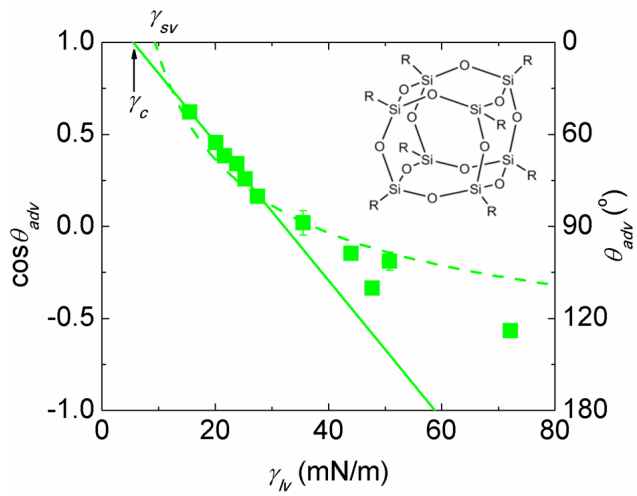
REC: Room 66-554, 77 Massachusetts Ave, Cambridge, MA 02139, Tel.: +1-617-253-3777; Fax: +1-617-258-8224, E-mail: recohen@mit.edu

GHM: Room 3-250, 77 Massachusetts Ave, Cambridge, MA 02139, Tel.: +1-617-258-0754; Fax: +1-617-258-8559, E-mail: gareth@mit.edu

ABSTRACT

The design of robust omniphobic surfaces, which are not wetted by low surface tension liquids such as octane ($\gamma_{lv} = 21.6$ mN/m) and methanol ($\gamma_{lv} = 22.7$ mN/m), requires an appropriately chosen surface micro/nano-texture in addition to a low solid surface energy (γ_{sv}). 1H,1H,2H,2H-Heptadecafluorodecyl polyhedral oligomeric silsesquioxane (fluorodecyl POSS) offers one of the lowest solid surface energy values ever reported ($\gamma_{sv} \approx 10$ mN/m) and has become the molecule of choice for coating textured surfaces. In this work, we synthesize and evaluate a series of related molecules that either retain the POSS cage and differ in fluoroalkyl chain length or that retain the fluorodecyl chains surrounding a linear or cyclic molecular structure. The solid surface energy (γ_{sv}) of these molecules was estimated using contact angle measurements on flat spin-coated silicon wafer surfaces. Zisman analysis was performed using a homologous series of n-alkanes ($15.5 \leq \gamma_{lv} \leq 27.5$ mN/m), while Girifalco-Good analysis was performed using a set of polar and non-polar liquids with a wider range of liquid surface tension ($15.5 \leq \gamma_{lv} \leq 72.1$ mN/m). The hydrogen bond donating, hydrogen bond accepting, polar and non-polar (dispersion) contributions to the solid surface energy of each compound were determined by probing the surfaces using a set of three liquid droplets of either acetone, chloroform and dodecane or diiodomethane, dimethyl sulfoxide and water.

SYNOPSIS TOC



KEYWORDS

Superhydrophobicity, oleophobicity, solid surface energy, Zisman analysis, Girifalco-Good method

Introduction

In the recent past, there have been a number of reports on surfaces that are not wetted by liquid droplets, *i. e.* superhydrophobic,¹⁻⁴ oleophobic,⁵⁻¹⁵ hydrophobic,¹⁶ omniphobic^{7, 12} surfaces. These surfaces have potential applications in oil-water separation, non-wettable textiles,^{2, 3, 6, 8, 9, 14, 15} and fingerprint/smudge resistant touch-screen devices. Here we use the term Omniphobicity to refer to surfaces that are not wetted by a broad set of liquids, including water, alkanes, alcohols, acids, bases and other organic liquids. The design of omniphobic surfaces involves selection of a suitable surface chemistry to minimize the solid surface energy and optimal choice of the surface texture.

In our previous work, we emphasized re-entrant topography as a necessary condition for the design of surfaces that are not wetted by low surface tension liquids.^{7-9, 11-13} Liquids such as octane ($\gamma_{lv} = 21.6$ mN/m) and methanol ($\gamma_{lv} = 22.7$ mN/m) will partially wet a flat untextured surface (equilibrium contact angle, $\theta_E < 90^\circ$) of any surface chemistry. Using a combination of surface chemistry and re-entrant texture, surfaces that exhibit substantially enhanced non-wettability to such liquids (apparent contact angle, $\theta^* > 90^\circ$) can be created. On such non-wetting surfaces, liquid droplets sit partially on the solid texture and partially on the air trapped between the asperities of the solid texture. The Cassie-Baxter (CB) relation can be used to understand variations in the apparent contact angles (θ^*) for liquid droplets with solid-liquid-air composite interfaces. The CB relation shows that the apparent contact angle (θ^*) increases as the equilibrium contact angle (θ_E) increases and as the relative amount of trapped air increases.¹⁷ We have also developed an expression for the breakthrough pressure (P_b) required for the disruption of this solid-liquid-air composite interface (or ‘CB state’).¹² Both the apparent contact angle (θ^*) and the breakthrough pressure (P_b) increase monotonically with increasing equilibrium contact angle (θ_E).^{7-9, 12} Therefore maximizing θ_E is one objective in the optimal design of omniphobic surfaces with robust composite interfaces.

We have used fluorodecyl POSS based coatings to design a range of robust non-wettable surfaces.^{7-9,}

¹¹⁻¹³ A fluorodecyl POSS molecule consists of a silicon – oxygen cage surrounded by eight

1H,1H,2H,2H-heptadecafluorodecyl chains.¹⁸ A flat silicon wafer spin-coated with a uniform coating of this molecule has one of the highest reported values of equilibrium contact angle for water droplets ($\theta_E \approx 122^\circ$). Moreover, liquid droplets with a wide range of surface tension ($15.5 \leq \gamma_{lv} \leq 72.1$ mN/m) form high contact angles on a fluorodecyl POSS coated flat surface (as summarized in **Figure 1**). The contact angles (θ_{adv} , and θ_{rec}) are significantly higher on a fluorodecyl POSS surface than on a corresponding surface coated with a fluoropolymer such as Tecnoflon (BR 9151, a fluoro-elastomer from Solvay Solexis). In addition, it is apparent from Figure 1 that the difference between the corresponding contact angles on the two surfaces *increases* as the liquid surface tension (γ_{lv}) *decreases*. The molecular level origins of the unusually low wettability of fluorodecyl POSS remains unresolved.

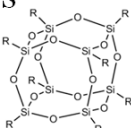
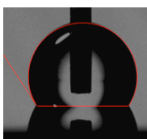
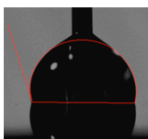
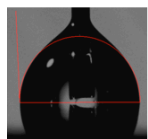
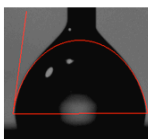
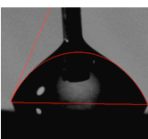
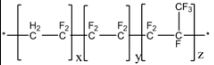
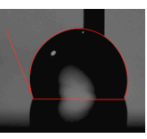
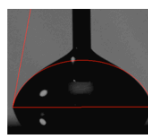
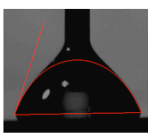
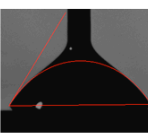
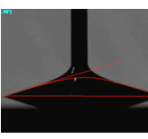
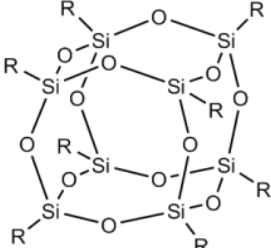
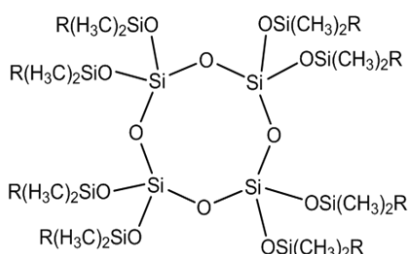
Advancing contact angles (θ_{adv})	Water ($\gamma_{lv} = 72.1$ mN/m)	Diiodomethane ($\gamma_{lv} = 50.8$ mN/m)	Rapeseed Oil ($\gamma_{lv} = 35.5$ mN/m)	Hexadecane ($\gamma_{lv} = 27.5$ mN/m)	Octane ($\gamma_{lv} = 21.6$ mN/m)
Fluorodecyl POSS 	$122 \pm 2^\circ$ 	$100 \pm 2^\circ$ 	$88 \pm 3^\circ$ 	$80 \pm 1^\circ$ 	$67 \pm 1^\circ$ 
Tecnoflon 	$110 \pm 2^\circ$ 	$80 \pm 2^\circ$ 	$71 \pm 2^\circ$ 	$58 \pm 2^\circ$ 	$16 \pm 3^\circ$ 

Figure 1. Variation of advancing contact angles (θ_{adv}) on flat silicon wafers spin-coated with fluorodecyl T_8 and Tecnoflon is shown. The advancing contact angles decrease in magnitude as the surface tension of the contacting liquids decreases from $\gamma_{lv} = 72.1$ mN/m (for water) to $\gamma_{lv} = 21.6$ mN/m (for octane) and as the solid surface energy increases from fluorodecyl T_8 to Tecnoflon.

In this study, we document the wettability of two sets of fluorinated silicon-containing molecules in an attempt to resolve some aspects of the unanswered questions regarding fluorodecyl POSS. In the first

set, the length of the fluorinated chain is changed keeping the T_8 silicon/oxygen cage intact. [This cage is referred to generally as the T_8 cage because it has eight silicon atoms each bonded to three oxygen atoms.] In the other set of molecules, the fluorodecyl chain is retained and the silicon/oxygen architecture is changed successively from a T_8 cage to a Q_4 ring [four Si atoms, each bonded to four oxygen atoms] or a M_2 straight chain [two Si atoms, each bonded to a single oxygen atom]. The structure and chemical formulae of various molecules are summarized in **Table 1**.

Table 1. Structure of Fluorohexyl T_8 , Fluoropropyl T_8 , Hexafluoro-*i*-butyl T_8 is shown along with the structure of Fluorodecyl T_8 and Fluorooctyl T_8 , Fluorodecyl Q_4 and Fluorodecyl M_2 for reference.

	Fluorodecyl T_8 , R = $-(\text{CH}_2)_2-(\text{CF}_2)_7-\text{CF}_3$
	Fluorooctyl T_8 , R = $-(\text{CH}_2)_2-(\text{CF}_2)_5-\text{CF}_3$
	Fluorohexyl T_8 , R = $-(\text{CH}_2)_2-(\text{CF}_2)_3-\text{CF}_3$
	Fluoropropyl T_8 , R = $-(\text{CH}_2)_2-\text{CF}_3$
	Hexafluoro- <i>i</i> -butyl T_8 , R = $-\text{CH}_2-\text{CH}(\text{CF}_3)_2$
	Fluorodecyl Q_4 , R = $-(\text{CH}_2)_2-(\text{CF}_2)_7-\text{CF}_3$
$\text{F}_3\text{C}(\text{F}_2\text{C})_7(\text{H}_2\text{C})_2(\text{H}_3\text{C})_2\text{Si}-\text{O}-\text{Si}(\text{CH}_3)_2(\text{CH}_2)_2(\text{CF}_2)_7\text{CF}_3$	Fluorodecyl M_2 , R = $-(\text{CH}_2)_2-(\text{CF}_2)_7-\text{CF}_3$

The wettability of these materials is assessed using contact angle measurements on smooth spin-coated Si wafers with a set of probing liquids. There are various methods described in the literature to estimate the solid surface energy from contact angle data: including the Zisman analysis,¹⁹ Owens-Wendt method,²⁰ or Girifalco-Good method^{21,22}. In this work, we perform Zisman analysis with a set of n-alkanes, a standard framework for quantifying non-wettability of low energy solid surfaces. We also estimate the surface energies of our solid surfaces using the Girifalco-Good analysis, which additionally considers polar contributions in the wettability analysis. **In the literature, the term “surface energy” is**

loosely used to indicate “surface energy per unit area” or “specific surface energy.” In this article, we have continued to use the term “surface energy” with the understanding that it indeed means “specific surface energy,” and it has units of mN/m or mJ/m².

Experimental Details

Fluorodecyl POSS: A 94.3% yield of pure 1H,1H,2H,2H-heptafluorodecyl₈T₈ (Fluorodecyl POSS) was obtained using a previously reported method.¹⁸

Fluorooctyl POSS: A 95.1% yield of pure 1H,1H,2H,2H-tridecafluorooctyl₈T₈ (Fluorooctyl POSS) was obtained using a previously reported method.¹⁸

Fluorohexyl POSS: A 91.5% yield of pure 1H,1H,2H,2H-nonafluorohexyl₈T₈ (Fluorohexyl POSS) was obtained using a previously reported method.¹⁸

Fluoropropyl POSS: Fluoropropyl POSS was synthesized using a modification of a previously reported method.²³ 3,3,3-Trifluoropropyltrichlorosilane (0.87 mL) was added to a stirred solution of heptakis(3,3,3-trifluoropropyl)tricycloheptasiloxane trisodium silanolate (4.00 g) in THF (70 mL) at room temperature. Triethylamine (0.49 mL) was then added drop wise to the mixture. The contents were stirred under nitrogen for 3 h in a 150 mL round bottom flask with a Teflon-coated magnetic stir bar. After filtering the precipitated salts, the filtrate was concentrated under reduced pressure. The fine white powder formed was rinsed with methanol and dried. A 76% yield of pure 3,3,3-trifluoropropyl₈T₈ (Fluoropropyl POSS) was obtained.

Hexafluoroisobutyl POSS: Hexafluoroisobutene (28.4 g, 173 mmole) was condensed into a 250 mL heavy walled reaction vessel with a Teflon-coated magnetic stir bar. HSiCl₃ (23.9 g, 176 mmol) was

then added at -10 °C under nitrogen followed by a 0.2 M H₂PtCl₆ isopropanol catalyst solution (0.5 mL, 0.1 mmol). The flask was sealed, heated to 150 °C, and stirred for 40 h. The contents were then vacuum transferred at 0 °C to a collection flask, which was then cooled to -80 °C. While slowly warming to -40 °C, volatiles were removed under static vacuum to give an 85 % yield of hexafluoroisobutyltrichlorosilane (44.2 g, 148 mmol). ¹H NMR (δ, CDCl₃) 3.29 ppm (1H, nonet, ³J_{H-F} and ³J_{H-H} = 7.2 Hz, CH), 1.93 ppm (2H, d, ³J_{H-H} = 7.2 Hz, CH₂); ¹⁹F NMR (δ, CDCl₃) -68.23 ppm (d, ³J_{H-F} = 7.2 Hz); ¹³C{¹H} NMR (δ, CDCl₃) 123.28 ppm (quart, ¹J_{C-F} = 281 Hz, CF₃) 44.40 ppm (sept, ²J_{C-F} = 30 Hz, CH), 18.49 (m, ³J_{C-F} = 1.8 Hz, CH₂); ²⁹Si{¹H} NMR (δ, CDCl₃) 8.14 ppm (br, s).

Hexafluoroisobutyltrichlorosilane (44.19 g, 148 mmole) was placed into a 250 mL round bottom flask (rbf) with a Teflon-coated magnetic stir bar under nitrogen and heated to 100 °C. Trimethylorthoformate (145.3 mL, 1.33 mol) was added drop-wise over a period of 1.5 h and the reaction was refluxed overnight. 1H,1H,2H-Hexafluoroisobutyltrimethoxysilane was isolated by fractional distillation (bp = 102 °C) under full dynamic vacuum, in 63 % isolated yield (26.57g, 93 mmol). ¹H NMR (δ, CDCl₃) 3.52 ppm (9 H, s, OMe), 3.06 ppm (1H, nonet, ³J_{H-F} and ³J_{H-H} = 7.2 Hz, CH), 0.97 ppm (2H, d, ³J_{H-H} = 7.2 Hz, CH₂); ¹⁹F NMR (δ, CDCl₃) -69.25 ppm (d, ³J_{H-F} = 7.2 Hz); ¹³C{¹H} NMR (δ, CDCl₃) 123.75 ppm (quart, ¹J_{C-F} = 269 Hz, CF₃), 50.27 (s, OCH₃) 43.64 ppm (sept, ²J_{C-F} = 29 Hz, CH), 3.20 (m, ³J_{C-F} = 1.7 Hz, CH₂); ²⁹Si{¹H} NMR (δ, CDCl₃) -48.7 ppm (s).

1H,1H,2H-Hexafluoroisobutyltrimethoxysilane (2.00 g, 7.00 mmole) and 205 mg of KOH solution (774 mg KOH in 100 mL H₂O) were added to 7 mL ethanol in a 25 mL rbf with a Teflon-coated magnetic stir bar and stirred overnight at room temperature, under nitrogen. The fine white powder formed was rinsed with ethanol and dried. An 85% yield of pure Hexafluoroisobutyl POSS was obtained. ¹H NMR (δ, C₆F₆) 3.65 ppm (1H, nonet, ³J_{H-F} and ³J_{H-H} = 7 Hz, CH), 1.54 ppm (2H, d, ³J_{H-H} = 7 Hz, CH₂); ¹⁹F NMR (δ, C₆F₆) -70.4 ppm (d, ³J_{H-F} = 7 Hz); ¹³C{¹H} NMR (δ, C₆F₆) 123.47 ppm (quart, ¹J_{C-F} = 282 Hz, CF₃), 43.83 ppm (sept, ²J_{C-F} = 30 Hz, CH), 5.18 (s, CH₂); ²⁹Si{¹H} NMR (δ, C₆F₆) -69.4 ppm (s).

1H,1H,2H,2H-Heptadecafluorodecyl₈M₈Q₄ (Fluorodecyl₈M₈Q₄): 1H,1H,2H,2H-Heptadecafluorodecyl dimethylchlorosilane (25 g, 46.2 mmol), octakis[chloro calcium oxy]cyclotetrasilicate²⁴ (3.4 g, 3.7 mmol), acetone (50 mL), and AK225 (14 mL) were added to a 100 mL rbf and refluxed under nitrogen for three days.²⁵ The volatiles were then removed under vacuum. The product was dissolved in AK225 solvent (50 mL) and a water extraction was used to remove CaCl₂. Isopropanol (10 mL) and Amberlyst 15 (1 g) were added after reducing the solvent to 25 mL. Amberlyst is a sulfonic acid catalyst based in a cross-linked styrene divinylbenzene polymeric resin. Amberlyst is commercially available, reusable, and non-hazardous. It works under heterogeneous conditions and can easily be removed by filtration. After 3 h of stirring, the solution was filtered through silica gel (1.20 g, 60 Å pore size, 35-75 micron particle size). After re-dissolving the product in AK225 (11 mL), Amberlyst 15 (1.03 g) and silica gel were added,²⁶ and the mixture was stirred overnight at room temperature. The solution was filtered through silica gel, the volatiles were removed by dynamic vacuum, and a distillation to isolate the fluorodecyl₂M₂ disiloxane was performed (see below). The fluorodecyl₈M₈Q₄ was dissolved in a minimal amount of AK225. A white precipitate formed upon sitting at room temperature. The AK225 was filtered off and the solid was washed with chloroform. A 9% yield (1.5 g) of fluorodecyl₈M₈Q₄ was obtained. ²⁹Si{¹H} NMR (AK225, ppm) 12.0 (s), -108.3 (s).

1,3-bis(1H,1H,2H,2H-Heptadecafluorodecyl)-1,3-tetramethyldisiloxane (Fluorodecyl₂M₂ disiloxane): A distillation at 118 °C, 0.2 mmHg was performed during the synthesis of Fluorodecyl₈M₈Q₄ to isolate fluorodecyl₂M₂ disiloxane. A 10% yield (4.7 g) of fluorodecyl₂M₂ disiloxane was obtained. ¹H NMR (CDCl₃, ppm) 0.12 (s), 0.75 (m), 2.03 (m). ²⁹Si{¹H} NMR (CDCl₃, ppm) 8.4 (s).

Surface characterization – The fluoroalkylated silicon-containing molecules were dissolved in Asahiklin solvent (AK 225, Asahi Glass Company) at a concentration of 10 mg/ml. Later, the solutions

were spin-coated on a flat silicon wafer at 900 rpm for 30 seconds to achieve uniformly coated flat surfaces (AFM rms roughness ~ 10 nm, [Table S7 and Figure S5 in the Supporting Information](#)) for contact angle measurements. Advancing and receding contact angles were measured using a VCA2000 goniometer (AST Inc.) with ~ 5 μL droplets of various liquids (purchased from Aldrich and used as received).

Results and Discussion

Zisman and co-workers introduced the concept of the critical surface tension for a solid surface (γ_c),^{19, 27-38} and it has become the most commonly used parameter to rank order solid surface energy (γ_{sv}) and wettability of different substrates. In order to assess the impact of molecular structure on wettability, contact angle measurements were performed on the full set of fluoroalkylated silicon containing molecules shown in **Table 1**. n-alkanes [pentane ($\gamma_{lv} = 15.5$ mN/m) to hexadecane ($\gamma_{lv} = 27.5$ mN/m)] were used as contacting liquids, and the advancing contact angles (θ_{adv}) results are summarized in **Figure 2**. Strong linear correlations ($R^2 = 0.95$ to 0.99) were observed for plots of $\cos\theta_{adv}$ versus liquid surface tension (γ_{lv}). The critical surface tension (γ_c) for the spin-coated surfaces was obtained by a linear extrapolation of the best-fit line through the $\cos\theta_{adv}$ versus γ_{lv} data. The intercept of this extrapolation to the $\cos\theta_{adv} = 1$ line is the critical surface tension (γ_c). As the length of the perfluorinated chain decreased from fluorodecyl T_8 (■) to fluoropropyl T_8 (◄), the critical surface tension (γ_c) increased monotonically from 5.5 to 19.7 mN/m. This trend is consistent with Zisman's results on modified poly tetrafluoroethylene (PTFE),³⁷ chlorinated polymers,³¹ fluorinated (meth)acrylate polymers,³⁵ and perfluorinated carboxylic acids.^{29, 33, 34} Additionally, the critical surface tension (γ_c) increased as the size and complexity of the $-\text{Si}/\text{O}-$ structure decreased; from $\gamma_c = 5.5$ mN/m for the fluorodecyl T_8 (cage, ■) to $\gamma_c = 14.5$ mN/m for the fluorodecyl Q_4 (ring, ▲) and $\gamma_c = 19.6$ mN/m for the fluorodecyl M_2 (straight chain, ▼).

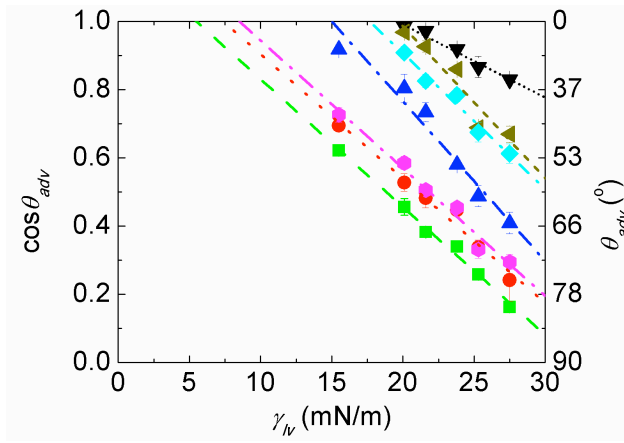


Figure 2. Zisman analysis for fluoroalkylated silicon-containing compounds. Cosine of advancing contact angles (θ_{adv}) for droplets of hexadecane ($\gamma_{lv} = 27.5$ mN/m), dodecane ($\gamma_{lv} = 25.3$ mN/m), decane ($\gamma_{lv} = 23.8$ mN/m), octane ($\gamma_{lv} = 21.6$ mN/m), heptane ($\gamma_{lv} = 20.1$ mN/m), and pentane ($\gamma_{lv} = 15.5$ mN/m) on a spin-coated film on a flat silicon wafer are plotted against the surface tension of contacting liquids (γ_{lv}). For fluoro-decyl T_8 ($\gamma_c = 5.5$ mN/m, ■), fluoro-octyl T_8 ($\gamma_c = 7.4$ mN/m, ●), fluoro-hexyl T_8 ($\gamma_c = 8.5$ mN/m, ◆), fluoro-propyl T_8 ($\gamma_c = 19.7$ mN/m, ▲), hexafluoroisbutyl T_8 ($\gamma_c = 17.7$ mN/m, ◆), fluoro-decyl Q_4 ($\gamma_c = 14.5$ mN/m, ▲), and fluoro-decyl M_2 ($\gamma_c = 19.6$ mN/m, ▼), the critical surface tension (γ_c) is obtained by a linear extrapolation of the corresponding best-fit line.

The critical surface tension (γ_c) is a qualitative indicator of the solid surface energy (γ_{sv}) but it is not equal to the solid surface energy ($\gamma_c \neq \gamma_{sv}$). Any liquid with a lower surface tension than the critical surface tension ($\gamma_{lv} < \gamma_c$) is expected to completely wet the solid surface ($\theta_E \approx 0$). Zisman noted that the critical surface tension (γ_c) can change if a different set of probing liquids is used on the same solid surface. When the solid surface and/or the contacting liquid is polar with a higher value of surface tension, the contact angle data deviates from the linear trend, as shown in **Figure 3** for a flat silicon wafer spin-coated with fluoro-decyl T_8 . The advancing contact angle data (θ_{adv} , ■) for liquids with a wider range of surface tensions ($15.5 \leq \gamma_{lv} \leq 72.1$ mN/m) are plotted along with the linear extrapolation of the Zisman line (—). The Zisman line fits the alkane data well ($R^2 = 0.99$ for fluoro-decyl T_8 , Figure 2, $\gamma_{lv} \leq 30$ mN/m), however it deviates significantly when other liquids are included ($R^2 = 0.04$

for fluorodecyl T_8 , Figure 3). Alkanes are completely non-polar, while higher surface tension liquids like water, ethylene glycol or dimethyl sulfoxide have polar functional groups and the polarity of these probing liquids is considered to be the cause of deviation from the Zisman line.

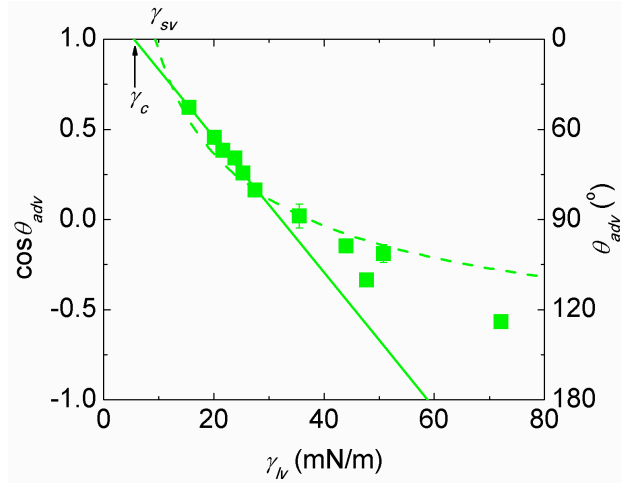


Figure 3. Variation of advancing contact angles (θ_{adv}) of liquid droplets with a wide range of surface tension on a fluorodecyl T_8 surfaces is shown in this figure. Cosine of advancing contact angles (θ_{adv}) for droplets of water ($\gamma_{lv} = 72.1$ mN/m), diiodomethane ($\gamma_{lv} = 50.8$ mN/m), ethylene glycol ($\gamma_{lv} = 47.7$ mN/m), dimethyl sulfoxide ($\gamma_{lv} = 44$ mN/m), rapeseed oil ($\gamma_{lv} = 35.5$ mN/m), hexadecane ($\gamma_{lv} = 27.5$ mN/m), dodecane ($\gamma_{lv} = 25.3$ mN/m), decane ($\gamma_{lv} = 23.8$ mN/m), octane ($\gamma_{lv} = 21.6$ mN/m), heptane ($\gamma_{lv} = 20.1$ mN/m), and pentane ($\gamma_{lv} = 15.5$ mN/m) on a spin-coated film on a flat silicon wafer are plotted against the surface tension of contacting liquids (γ_{lv}). The Zisman best fit line for the alkane data (—) and the best fit Girifalco-Good curve (- - -) over the whole range of liquids is shown with the respective intercepts $\gamma_c = 5.5$ mN/m, and $\gamma_{sv} = 9.3$ mN/m respectively.

A better model which incorporates the polarity of the solid surface and/or the contacting liquid was proposed by Girifalco, Good and co-workers.^{21, 22, 39-43} According to this framework, the solid surface energy (γ_{sv}) is given by Equation 1, where θ_E is the equilibrium contact angle and ϕ_{sl} is a solid-liquid interaction parameter.

$$W_{sl}^a = \gamma_{lv} (1 + \cos \theta_E) = 2\phi_{sl} \sqrt{\gamma_{sv} \gamma_{lv}} \quad (1)$$

Equation 1 has two unknowns, γ_{sv} and ϕ_{sl} . The parameter ϕ_{sl} equals the ratio of work of adhesion of the solid-liquid pair (W_{sl}^a) to the square roots of the works of cohesion of the solid ($W_{ss}^c = 2\gamma_{sv}$) and the liquid ($W_{ll}^c = 2\gamma_{lv}$), where $W_{ss}^c W_{ll}^c = 4\gamma_{sv}\gamma_{lv}$. The Berthelot geometric mean mixing rule suggests that the work of adhesion can be approximated as the product of the square roots of the two works of cohesion.²² For non-polar liquid droplets on non-polar solids, this is indeed the case ($W_{sl}^a = \sqrt{W_{ss}^c W_{ll}^c}$), and the solid-liquid interactions are nearly ideal ($\phi_{sl} = W_{sl}^a / \sqrt{W_{ss}^c W_{ll}^c} = 1$), *e. g.* alkane droplets on fluorodecyl POSS (Figure 2 and 3). However, in general, the value of ϕ_{sl} for a solid/liquid pair is not known *a priori*. Contact angle measurements were performed over a broad range of liquids with differing polarities and the average value of ϕ_{sl} was assumed to be unity. The advancing contact angle measurement results, along with the ($\phi_{sl} = 1$) best fit Girifalco-Good curve (— — —) are shown in Figure 3 for a fluorodecyl T_8 surface. Alkanes from pentane ($\gamma_{lv} = 15.5$ mN/m) to hexadecane ($\gamma_{lv} = 27.5$ mN/m), rapeseed oil ($\gamma_{lv} = 35.5$ mN/m), and diiodomethane ($\gamma_{lv} = 50.8$ mN/m) represent a set of non-polar liquids; whereas dimethyl sulfoxide ($\gamma_{lv} = 44$ mN/m), ethylene glycol ($\gamma_{lv} = 47.7$ mN/m) and water ($\gamma_{lv} = 72.1$ mN/m) have polar nature. When compared with the extrapolated Zisman line (———, $R^2 = 0.04$), the Girifalco-Good curve (— — —) is a much better fit ($R^2 = 0.88$) to the advancing contact angle data over the whole range of liquid surface tensions, barring the two outliers – water ($\gamma_{lv} = 72.1$ mN/m) and ethylene glycol ($\gamma_{lv} = 47.7$ mN/m), which lie significantly below the curve. Statistical analysis based on the residuals between the best-fit predictions and measured values of $\cos\theta_{adv}$ are summarized in the supporting information (Figure S1 and S2).

One of the main sources of uncertainty with Zisman analysis is the large extrapolation of the best-fit line to $\theta_{adv} \square 0$ that is typically required to estimate the value of γ_c . In the Girifalco-Good analysis, such an extrapolation is avoided. If a liquid (with surface tension γ_{lv}^*) is found such that it forms an equilibrium contact angle, $\theta_E \approx 90^\circ$, then assuming that $\phi_{sl} = 1$, the solid surface energy can be found by solving Equation 1 which yields $\gamma_{sv} = \gamma_{lv}^*/4$. Even if such a liquid cannot be found, γ_{sv} can be estimated

by interpolation using two liquids (say 1 and 2) if $\theta_{E,1} > 90^\circ$ and $\theta_{E,2} < 90^\circ$. The location, shape and curvature of the Girifalco-Good curve are an embodiment of the solid surface energy (γ_{sv}), and in Zisman analysis, it is γ_c . The solid surface energy (γ_{sv}) can also be represented as the intercept where the extrapolated Girifalco-Good curve intersects the $\cos\theta_{adv} = 1$ line [$\gamma_{sv} = 9.3$ mN/m in this case].

Since the Girifalco-Good curve has positive curvature (*i.e.* it is concave ‘upwards’), the Zisman critical surface tension always tends to underestimate the solid surface energy ($\gamma_c < \gamma_{sv}$) determined from Girifalco-Good analysis. The Girifalco-Good relation (Equation 1) can be re-written in the form $\cos\theta_E = -1 + 2\phi_{sl}\sqrt{\gamma_{sv}/\gamma_{lv}}$, which can be further expressed as a Taylor series when $\gamma_{lv}/\gamma_{sv} \rightarrow 1^+$ in terms of $(\gamma_{lv}/\gamma_{sv} - 1)$, as shown in Equation 2 (assuming $\phi_{sl} = 1$, a good assumption for alkanes).²²

$$\cos\theta_E = 1 - \left(\frac{\gamma_{lv}}{\gamma_{sv}} - 1\right) + \frac{3}{4}\left(\frac{\gamma_{lv}}{\gamma_{sv}} - 1\right)^2 - \frac{5}{8}\left(\frac{\gamma_{lv}}{\gamma_{sv}} - 1\right)^3 + \frac{35}{64}\left(\frac{\gamma_{lv}}{\gamma_{sv}} - 1\right)^4 - \dots \quad (2)$$

This series converges only if $(\gamma_{lv}/\gamma_{sv} - 1) < 1$ *i.e.* $\gamma_{lv} < 2\gamma_{sv}$. The Taylor series can be truncated after the second term to get a linear relation between $\cos\theta_E$ and γ_{lv} (Equation 3), and the absolute value of the slope of this line is expected to be the inverse of the solid surface energy (γ_{sv}).

$$\cos\theta_E \approx 1 - \left(\frac{\gamma_{lv}}{\gamma_{sv}} - 1\right) \quad (3)$$

This linearization is valid only if the quadratic term is considerably smaller (ca 10%) compared to the linear term. This condition restricts the range of liquid surface tensions $(\gamma_{lv}/\gamma_{sv}) < 1.13$ for which the linearization is valid, therefore in general, this linearization should be avoided. Johnson and Dettre have reported the value of the Zisman slope along with the intercept (γ_c) as a more complete indicator of the solid surface energy.⁴⁴ The absolute value of the Zisman slope equals the reciprocal of the Zisman critical surface tension (*i.e.* $\partial \cos\theta_E / \partial \gamma_{lv} = -1/\gamma_{sv}$). Slopes in the range of -0.035 to -0.050 (mN/m)⁻¹ were reported and the absolute value of the slope tends to increase with increasing γ_c .⁴⁴ This trend is contradictory to the linear form of the truncated Taylor series expansion of the Girifalco-Good equation.

Therefore, the slope of the Zisman line does not provide a complete description of the solid surface energy (γ_{sv}).

The Girifalco-Good framework was also applied to smooth spin-coated surfaces prepared from the other T_8 molecules and the values of the solid surface energy (γ_{sv}) were computed from the advancing contact angle data (**Figure 4**). The calculated values of the solid surface energy monotonically increase from $\gamma_{sv} = 9.3$ to 18.7 mN/m as the length of the fluorinated side chain decreases from fluorodecyl T_8 (■) to fluoropropyl T_8 (◄). These values follow a similar trend to that of the critical surface tension (γ_c), but as expected, there is a lack of quantitative agreement between the two.

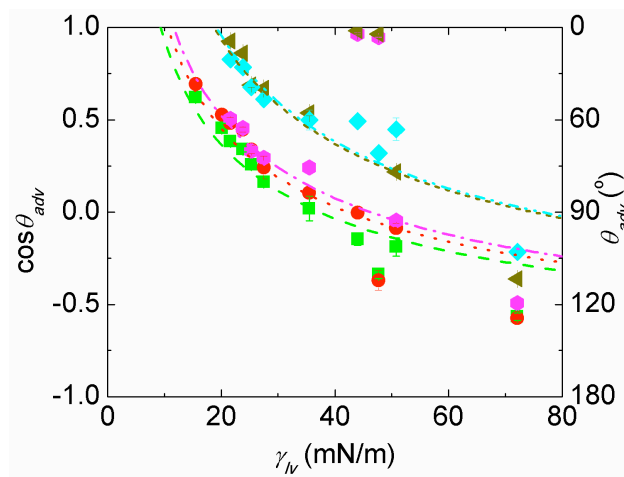


Figure 4. Variation of advancing contact angles (θ_{adv}) for T_8 cages surrounded by various fluorinated chains is summarized in this figure. Cosine of advancing contact angles (θ_{adv}) for droplets of water ($\gamma_{lv} = 72.1$ mN/m), diiodomethane ($\gamma_{lv} = 50.8$ mN/m), ethylene glycol ($\gamma_{lv} = 47.7$ mN/m), dimethyl sulfoxide ($\gamma_{lv} = 44$ mN/m), rapeseed oil ($\gamma_{lv} = 35.5$ mN/m), hexadecane ($\gamma_{lv} = 27.5$ mN/m), dodecane ($\gamma_{lv} = 25.3$ mN/m), decane ($\gamma_{lv} = 23.8$ mN/m), octane ($\gamma_{lv} = 21.6$ mN/m), heptane ($\gamma_{lv} = 20.1$ mN/m), and pentane ($\gamma_{lv} = 15.5$ mN/m) on a spin-coated film on a flat silicon wafer are plotted against the surface tension of contacting liquids (γ_{lv}). Solid surface energy for Fluorodecyl T_8 ($\gamma_{sv} = 9.3$ mN/m, ■), fluoroethyl T_8 ($\gamma_{sv} = 10.6$ mN/m, ●), fluoroethyl T_8 ($\gamma_{sv} = 11.6$ mN/m, ◆), fluoropropyl T_8 ($\gamma_{sv} = 18.7$ mN/m, ◄), and hexafluoroisbutyl T_8 ($\gamma_{sv} = 19.1$ mN/m, ◆) is estimated by the extrapolation of the best fit Girifalco-Good curve.

A close packed monolayer of $-\text{CF}_3$ moieties has the lowest known solid surface energy ($\gamma_{sv} \approx 6.7 \text{ mN/m}$).^{19, 45} The side-chains of the fluoroalkylated molecules under consideration terminate with $-\text{CF}_3$ groups which are backed by $-\text{CF}_2-$ groups, with surface energies in the range of $\gamma_{sv} \approx 18$ - 20 mN/m .³⁶ As the length of the perfluorinated chain increases, close packing of the chains becomes more favorable and consequently liquid-induced molecular reorganization at the surface becomes restricted. For fluorodecyl T_8 with the longest perfluorinated chain (seven $-\text{CF}_2-$ groups), predominantly $-\text{CF}_3$ groups are presented at the surface and the surface energy remains quite low ($\gamma_{sv} = 9.3 \text{ mN/m}$). However, as the length of the fluorinated chain decreases, the tendency to chain alignment and crystallization reduces and the chains at the solid-liquid interface become more susceptible to liquid-induced reorganization. Consequently, the underlying higher surface energy moieties ($-\text{CF}_2-$ and $-\text{CH}_2-$ groups) are exposed to the contacting liquid, and γ_{sv} increases significantly from the value $\gamma_{sv} = 9.3 \text{ mN/m}$, which is close to that of a $-\text{CF}_3$ monolayer.

It was also noted that some high surface tension liquids like dimethyl sulfoxide ($\gamma_{lv} = 44 \text{ mN/m}$) or ethylene glycol ($\gamma_{lv} = 47.7 \text{ mN/m}$) fully wet ($\theta_E \square 0^\circ$) the fluorohexyl and fluoropropyl T_8 surfaces, even though $\gamma_{lv} \gg \gamma_c$. This unexpected behavior is due to specific polar interactions across the solid-liquid interface and it can be understood by careful examination of the Girifalco-Good framework.

In one set of molecules, the T_8 cage structure was kept constant and the length of the perfluorinated side chain was changed (Figure 4). It was found that fluorodecyl T_8 , with the longest perfluorinated side chain, had the lowest solid surface energy (γ_{sv}) among the T_8 molecules. Therefore, in a second set of molecules, the fluorodecyl side chain was kept constant but the $-\text{Si/O}-$ architecture was changed from the T_8 cage (■) to a Q_4 ring (▲) as well as a linear chain molecule (▼, M_2). The solid surface energy (γ_{sv}) increased from 9.3 mN/m for the fluorodecyl T_8 , to 14.3 mN/m for fluorodecyl Q_4 , and finally to 26.8 mN/m for fluorodecyl M_2 (Figure 5). This trend is consistent with the variation in the corresponding critical surface tensions (γ_c) obtained from Zisman analysis. In this set of molecules, the

perfluorinated side chain was held constant; therefore changes in the $-\text{Si}/\text{O}-$ architecture are the only possible cause for the change in wettability. For the fluorodecyl M_2 molecules, the relative ease of access to the high surface energy $-\text{Si}-\text{O}-\text{Si}-$ moiety is expected to be the reason for its high solid surface energy. The reason for the difference in wettability of the fluorodecyl T_8 and Q_4 molecules is provisionally attributed to the presence of the $-\text{Si}/\text{O}-$ cage.

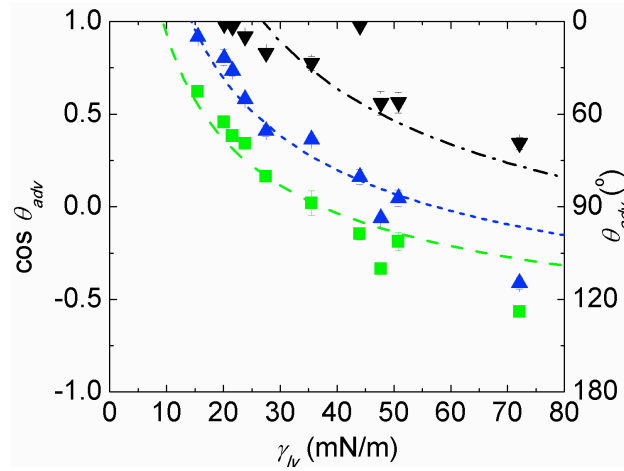


Figure 5. Variation of advancing contact angles (θ_{adv}) for various $-\text{Si}/\text{O}-$ moieties surrounded by $1H,1H,2H,2H$ -heptadecafluorodecyl chains is summarized. Cosine of advancing contact angles (θ_{adv}) for droplets of water ($\gamma_{lv} = 72.1$ mN/m), diiodomethane ($\gamma_{lv} = 50.8$ mN/m), ethylene glycol ($\gamma_{lv} = 47.7$ mN/m), dimethyl sulfoxide ($\gamma_{lv} = 44$ mN/m), rapeseed oil ($\gamma_{lv} = 35.5$ mN/m), hexadecane ($\gamma_{lv} = 27.5$ mN/m), dodecane ($\gamma_{lv} = 25.3$ mN/m), decane ($\gamma_{lv} = 23.8$ mN/m), octane ($\gamma_{lv} = 21.6$ mN/m), heptane ($\gamma_{lv} = 20.1$ mN/m), and pentane ($\gamma_{lv} = 15.5$ mN/m) on a spin-coated film on a flat silicon wafer are plotted against the surface tension of contacting liquids (γ_{lv}). Solid surface energy for Fluorodecyl T_8 ($\gamma_{sv} = 9.3$ mN/m, \blacksquare), fluorodecyl Q_4 ($\gamma_{sv} = 14.3$ mN/m, \blacktriangle), and fluorodecyl M_2 ($\gamma_{sv} = 26.8$ mN/m, \blacktriangledown) is estimated by the extrapolation of the best fit Girifalco-Good curve.

According to the Girifalco – Good framework, the total surface energy can be divided into a dispersion (or non-polar, γ^d) and a polar (γ^p) component. Subsequently, Girifalco, Good and co-workers

expressed the polar component of a solid (γ_{sv}^p) or a liquid (γ_{lv}^p) in terms of hydrogen bond donating (or acidic, γ^+) and hydrogen bond accepting (or basic, γ^-) components (as shown in Equation 4).

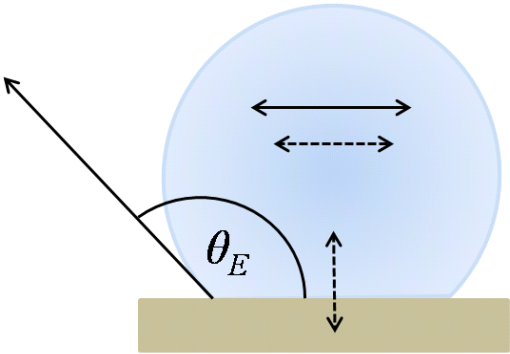
$$\begin{aligned}\gamma_{lv} &= \gamma_{lv}^d + \gamma_{lv}^p = \gamma_{lv}^d + 2\sqrt{\gamma_{lv}^+ \gamma_{lv}^-} \\ \gamma_{sv} &= \gamma_{sv}^d + \gamma_{sv}^p = \gamma_{sv}^d + 2\sqrt{\gamma_{sv}^+ \gamma_{sv}^-}\end{aligned}\quad (4)$$

Liquids such as acetone ($\gamma_{lv} = 25.2$ mN/m) or dimethyl sulfoxide ($\gamma_{lv} = 44$ mN/m) have an oxygen atom attached to an electropositive atom; therefore, the oxygen can donate its lone pair of electrons or accept hydrogen bonds. These liquids do not have any acidic protons, and therefore have negligibly small values of hydrogen bond donating components of surface energy (γ_{lv}^+). Such liquids with one predominant polar component are said to be monopolar liquids. Liquids like ethylene glycol ($\gamma_{lv} = 47.7$ mN/m) and glycerol ($\gamma_{lv} = 66$ mN/m) have both (a) an electronegative atom like oxygen which can accept hydrogen bonds, and (b) a hydrogen atom bonded to electronegative oxygen atom, which can be easily donated. Therefore, such liquids have appreciable values of both the polar components ($\gamma_{lv}^+, \gamma_{lv}^-$), and they are commonly termed bipolar liquids. Values of the surface energy components are known (tabulated in the supporting information) based on water as a standard state with $\gamma_{lv}^+ = \gamma_{lv}^- = 25.5$ mN/m. Some researchers have recently argued that for water $\gamma_{lv}^+ / \gamma_{lv}^- = 6.5$, based on the shifts in the absorption wavelengths of solvatochromic dyes,⁴⁶ but we have used the former standard state due to the availability of surface energy component data in this reference frame. Finally, it is important to note that the magnitude of acidic (γ_{sv}^+) and basic components (γ_{sv}^-) of the solid surface energy depends on the choice of the standard state, whereas the magnitude of the total polar ($\gamma_{sv}^p = 2\sqrt{\gamma_{sv}^+ \gamma_{sv}^-}$) and dispersion component (γ_{sv}^d) is independent of the standard state.

Two molecules of a bipolar liquid can have dispersion (non-polar) as well as polar cohesive interactions with each other; and due to the presence of these additional polar interactions, the surface tension (γ_{lv}) and work of cohesion ($W_{ll}^c = 2\gamma_{lv}$) for bipolar liquids tends to be higher than for non-polar or monopolar liquids (**Figure 6**). A droplet of a bipolar liquid can interact with a non-polar solid only

through dispersion adhesive interactions, and consequently the work of adhesion (W_{sl}^a) tends to be lower for a bipolar liquid on a non-polar solid. Therefore, for a droplet of bipolar liquid (like water and ethylene glycol) on a non-polar solid, the parameter $\phi_{sl} = W_{sl}^a / \sqrt{W_{ss}^c W_{ll}^c} < 1$.⁴⁷ In Figure 3, 4 and 5, we fitted Equation 1 to the advancing contact angle data, assuming $\phi_{sl} = 1$, but we now recognize that $\phi_{sl} < 1$ for water and ethylene glycol on non-polar surfaces. Therefore, these points corresponding to bipolar liquids are not expected to lie on the best-fit curve (Equation 1). The statistical Dixon Q-test was used to decide whether to use the water and/or ethylene glycol data for fitting Equation 1. Based on the magnitude of the residuals and the Q-test tables, both water and ethylene glycol data were rejected for fitting Equation 1 with a 95% confidence for the fluorodecyl T_8 surface. A similar statistical exercise was carried out for all the solid surfaces and the “best-fit” plots in Figure 4 and 5 are based on the liquids which satisfy the Dixon Q-test with 95% confidence (data shown in supporting information). Moreover from the value of the best-fit predicted and experimentally measured contact angles, the parameter ϕ_{sl} can be computed to be 0.60 for water and 0.75 for ethylene glycol on the fluorodecyl T_8 surface. For monopolar or non-polar liquids on non-polar solids, both the cohesive and adhesive interactions are dispersive, therefore the parameter ϕ_{sl} is expected to be close to unity and it is found to be $0.95 \leq \phi_{sl} \leq 1.05$ for such liquids on non-polar solids.

(a) Bipolar liquid on a non-polar solid ($\phi_{sl} < 1$)



(b) Monopolar or non-polar liquid on a non-polar solid ($\phi_{sl} \approx 1$)

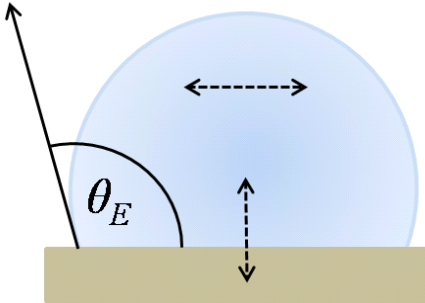


Figure 6. Schematic of (a) a bipolar and (b) a monopolar or a non-polar liquid droplet on a non-polar solid surface is shown. The dotted arrows ($\leftarrow - \rightarrow$) indicate a non-polar (dispersion) interaction and the filled arrows ($\leftarrow \rightarrow$) indicate a polar interaction. A bipolar liquid has both polar and non-polar cohesive interactions whereas a monopolar or a non-polar liquid has only non-polar cohesive interactions. Consequently, for the same values of liquid surface tension (γ_{lv}) and solid surface energy (γ_{sv}), a droplet of a bipolar liquid forms higher equilibrium contact angle (θ_E) compared to a droplet of either a monopolar or a non-polar liquid. (This figure is adapted from the book by Van Oss.⁴⁷)

The advancing contact angles for dimethyl sulfoxide and ethylene glycol droplets were found to have surprisingly low contact angles ($\theta_{adv} < 15^\circ$) on fluorohexyl T_8 , fluoropropyl T_8 , and fluorodecyl M_2 surfaces (Figure 4 and 5). These low contact angles are believed to occur due to a strong specific polar interaction ($\phi_{sl} \gg 1$) across the solid-liquid interface. These anomalously low contact angles were excluded from the fitting to obtain the solid surface energies. If a solid is soluble in a probing liquid, the contact angles of such a solid-liquid combination cannot be used for the estimation of solid surface energy (γ_{sv}). Solid-liquid pairs for which solubility is questionable are marked in red in Table S4 and S5 in the supporting information. However, we feel that probing a solid surface using a set of polar and non-polar liquids is a good approach to estimate solid surface energy (γ_{sv}).

The solid-liquid work of adhesion (W_{sl}^a) can be written in terms of the individual components of the surface energy of the solid and contacting liquid^{39, 42, 43}

$$W_{sl}^a = \gamma_{lv} (1 + \cos \theta_E) = 2 \left[\sqrt{\gamma_{sv}^d \gamma_{lv}^d} + \sqrt{\gamma_{sv}^+ \gamma_{lv}^-} + \sqrt{\gamma_{sv}^- \gamma_{lv}^+} \right] \quad (5)$$

Note that the first term on the right hand side of Equation 5 ($\sqrt{\gamma_{sv}^d \gamma_{lv}^d}$) has the same form as Equation 1, but the other two terms appear in the form of a cross product. The hydrogen bond donating component of the solid (γ_{sv}^+) interacts with the hydrogen bond accepting component of the liquid (γ_{lv}^-) and vice versa. If either the solid or the liquid is purely non-polar, then these polar interactions vanish and

Equation 5 simplifies to Equation 1. The individual contributions to the liquid surface tension ($\gamma_{lv}^d, \gamma_{lv}^+, \gamma_{lv}^-$) are known for a few standard liquids (See supporting information). Therefore by measuring the equilibrium contact angles of (at least) three contacting liquid droplets, the three unknowns in Equation 5 ($\gamma_{sv}^d, \gamma_{sv}^+, \gamma_{sv}^-$) can be obtained by solving a linear system of three equations $[A][x]=[b]$, given by Equation 6.

$$2 \begin{bmatrix} \sqrt{\gamma_{lv,1}^d} + \sqrt{\gamma_{lv,1}^-} + \sqrt{\gamma_{lv,1}^+} \\ \sqrt{\gamma_{lv,2}^d} + \sqrt{\gamma_{lv,2}^-} + \sqrt{\gamma_{lv,2}^+} \\ \sqrt{\gamma_{lv,3}^d} + \sqrt{\gamma_{lv,3}^-} + \sqrt{\gamma_{lv,3}^+} \end{bmatrix} \begin{bmatrix} \gamma_{sv}^d \\ \gamma_{sv}^+ \\ \gamma_{sv}^- \end{bmatrix} = \begin{bmatrix} \gamma_{lv,1} (1 + \cos \theta_{E,1}) \\ \gamma_{lv,2} (1 + \cos \theta_{E,2}) \\ \gamma_{lv,3} (1 + \cos \theta_{E,3}) \end{bmatrix} \quad (6)$$

The relative error in the contact angle measurements (the right hand side of Equation 6) is amplified by the condition number of matrix $[A]$, therefore the contacting liquids are chosen such that the matrix $[A]$ is not ill-conditioned or it has as low a condition number as possible.^{46, 48} Dodecane ($\gamma_{lv} = 25.3$ mN/m), chloroform ($\gamma_{lv} = 27.5$ mN/m), and acetone ($\gamma_{lv} = 25.2$ mN/m) were chosen as a set of contacting liquids. All the three liquids have similar values of surface tensions but different polarities. Acetone has a strongly monopolar hydrogen bond accepting component ($\gamma_{lv}^+ = 0, \gamma_{lv}^- = 24$ mN/m), and chloroform has a weakly monopolar hydrogen bond donating component ($\gamma_{lv}^+ = 3.8, \gamma_{lv}^- = 0$ mN/m), whereas dodecane is completely non-polar ($\gamma_{lv}^+ = \gamma_{lv}^- = 0$). Even though both acetone and chloroform are polar, due to their monopolar nature, the polar component of surface energy is zero ($\gamma_{lv}^p = 2\sqrt{\gamma_{lv}^+ \gamma_{lv}^-} = 0$). The condition number of the pre-factor matrix $[A]$ is reasonably small (7.2), therefore this set of liquids can be used successfully to evaluate the individual components of the solid surface energy. All three liquids are expected to have similar contact angles on non-polar solids (*i.e.* solids with $\gamma_{sv}^+ = \gamma_{sv}^- = 0$), as the last two terms of Equation 5 vanish and the interactions across solid-liquid are purely dispersive. Indeed, dodecane ($\theta_{adv} = 75 \pm 2^\circ$, $\theta_{rec} = 60 \pm 4^\circ$, \square), acetone ($\theta_{adv} = 71 \pm 2^\circ$, $\theta_{rec} = 59 \pm 4^\circ$, \square), and chloroform droplets ($\theta_{adv} = 73 \pm 2^\circ$, $\theta_{rec} = 54 \pm 4^\circ$, \square) all form similar contact angles on fluorodecyl T_8 , which is a completely non-polar molecule (**Figure 7(a)**). As the polarity of the surfaces increases from

fluorodecyl T_8 to fluoroocetyl T_8 , and finally fluorodecyl Q_4 , the acetone and chloroform droplets form much lower contact angles in comparison with dodecane droplets. For example, on the fluorodecyl Q_4 surface (Figure 7(c)), the dodecane contact angles ($\theta_{adv} = 62 \pm 2^\circ$, $\theta_{rec} = 17 \pm 2^\circ$, \blacktriangle) are much larger than those measured for acetone ($\theta_{adv} = 30 \pm 1^\circ$, $\theta_{rec} \approx 0^\circ$, \triangle) or chloroform ($\theta_{adv} = 29 \pm 4^\circ$, $\theta_{rec} = 15 \pm 3^\circ$, \blacktriangle). Therefore, it is vital to know about the polarity of the contacting liquids and solids when evaluating the equilibrium contact angles and solid surface energies (γ_{sv}).

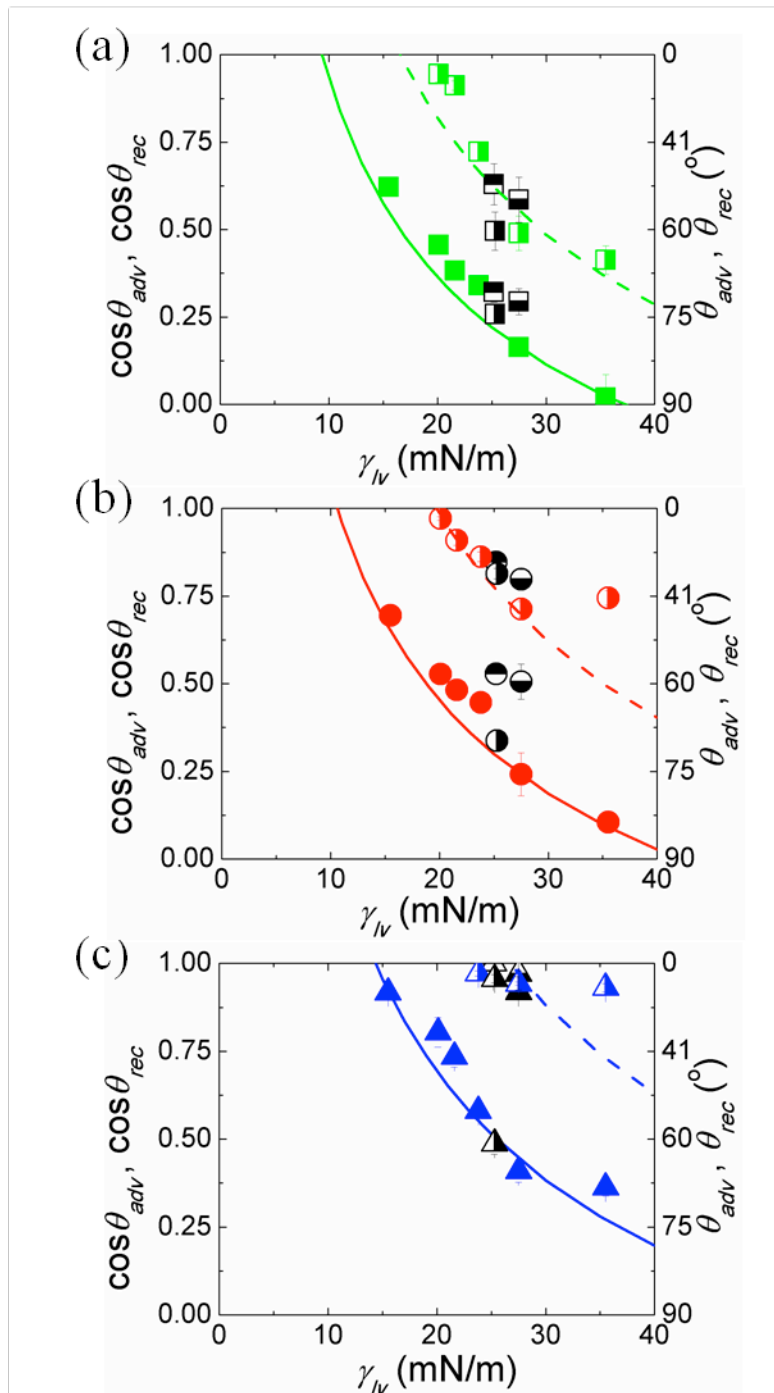


Figure 7. Variation of advancing and receding contact angles (θ_{adv} , θ_{rec}) is summarized for (a) fluorodecyl T_8 (■, □), (b) fluoroctyl T_8 (●, ○), and (c) fluorodecyl Q_4 (▲, △). Cosine of advancing and receding contact angles (θ_{adv} , θ_{rec}) for droplets of hexadecane ($\gamma_{lv} = 27.5$ mN/m), dodecane ($\gamma_{lv} = 25.3$ mN/m), decane ($\gamma_{lv} = 23.8$ mN/m), octane ($\gamma_{lv} = 21.6$ mN/m), heptane ($\gamma_{lv} = 20.1$ mN/m), pentane ($\gamma_{lv} = 15.5$ mN/m), chloroform ($\gamma_{lv} = 27.5$ mN/m), and acetone ($\gamma_{lv} = 25.2$ mN/m) on a spin-coated film on a flat silicon wafer are plotted against the surface tension of contacting liquids (γ_{lv}). Solid surface energy is estimated by substituting the values of the contact angles with dodecane (□, ○, △), chloroform (■) and acetone droplets (□) in the Girifalco – Good equation and summarized in Table 1.

Highly fluorinated species possess surfaces with relatively low polarity and low solid surface energy. The reason for this can be understood by looking at the unusual characteristics of fluorine. Fluorine is the most electronegative element of the periodic table (3.98 on the Pauling scale). Carbon (2.55) is significantly less electronegative. Consequently, a C–F bond is polar ($C^{\delta+} - F^{\delta-}$) and acquires partial ionic character. A carbon atom bonded to three fluorine atoms ($-CF_3$) is significantly electron deficient. The only way to reduce the dipole moment between this α carbon ($-CF_3$) and the adjacent β carbon is by placing electronegative atoms on the β carbon as well. By perfluorinating a large number of successive carbon atoms, the $-CF_2-CH_2-$ dipole is buried deep within the molecule. Therefore, fluorodecyl T_8 and other molecules with long fluorinated side chains exhibit an almost negligible polar component of solid surface energy ($\gamma_{sv}^p \approx 0$). Furthermore, due to the small size (van der Waals radius, $r = 1.47$ Å), the polarizability of a fluorine atom is small, and it is difficult to create fluctuating dipoles involving fluorine atoms. The interaction energy arising from London forces varies as the square of the polarizability. Therefore, the dispersion component of the solid surface energy (γ_{sv}^d) is also small for fluorinated species.⁴⁹ Intuitively, the high electronegativity of fluorine makes it an ideal candidate for accepting hydrogen bonds and fluorinated species might be expected to have a high value of γ_{sv}^- .

However, in practice, due to the small size and small polarizability, a fluorine atom holds the three lone pairs of electrons extremely tightly and is a poor hydrogen bond acceptor. The hydrogen bonds formed by fluorinated species are weaker in strength (typically 1/4th of the bond energy of a $-\text{C}=\text{O}\cdots\text{H}-\text{OR}$ bond).⁵⁰ On the contrary, hydrogen (2.20) and carbon (2.55) have similar electronegativities and form non-polar bonds. Due to the relatively higher polarizability of hydrogen, the dispersion component of the solid surface energy for hydrocarbons tends to be higher than corresponding fluorocarbons.

Using Equation 5 and the set of three liquids mentioned above (acetone, chloroform and dodecane), the solid surface energy was estimated for various fluoroalkylated silicon-containing molecules (summarized in **Table 2**). For the fluorodecyl T_8 POSS cages, this value of surface energy agreed (within experimental error) with the value estimated using Equation 1. However, the three probing liquids possess low surface tension values ($\gamma_{lv} \approx 25$ to 27 mN/m) and wet most non-fluorinated surfaces with values of $\gamma_{sv} > 25$ mN/m. Moreover, the relative error in the measurement of small contact angles is always large. Therefore, a set of probing liquids with higher surface tension values is needed to accurately probe higher energy surfaces. Water ($\gamma_{lv} = 72.1$ mN/m), diiodomethane ($\gamma_{lv} = 50.8$ mN/m), and dimethyl sulfoxide ($\gamma_{lv} = 44$ mN/m) constitute such a set with high values of liquid surface tension (and give rise to a small condition number for the matrix $[A]$, $\text{cond}(A) = 4.58$). Using this set of liquids, a broader range of surfaces ($\gamma_{sv} < 40$ mN/m) can be analyzed using the Girifalco-Good method (see Table 2 and **Table 3**). For fluorohexyl, fluoropropyl and hexafluoro-*i*-butyl T_8 surfaces, solid surface energy values obtained using these three high surface tension liquids (column 4 of Table 2) did not match the previously obtained values (columns 2 and 3). In order to diagnose the reason for this mismatch, the magnitudes of the individual components of the solid surface energy must be considered (as summarized in Table 3). The values of the dispersion component of the solid surface energy (γ_{sv}^d , given in column 5 of Table 3) match well with the solid surface energy (γ_{sv} , column 3 of Table 3) calculated using Equation 1.

Table 2. Computed values of solid surface energy (γ_{sv} mN/m) for various fluoroalkylated silicon containing moieties are summarized.

γ_{sv} (mN/m) based on contact angles ($^\circ$) of the probing liquids	All liquids* (Equation 1 with $\phi_{sl} = 1$)	Dodecane, acetone, and chloroform (Equation 5)	Diiodomethane, dimethyl sulfoxide and water (Equation 5)
Fluorodecyl T_8	9.3	10.2	8.8
Fluorooctyl T_8	10.6	13.6	10.9
Fluorohexyl T_8	11.6	26.8	47.4
Fluoropropyl T_8	18.7	21.4	38.4
Hexafluoro-<i>i</i>-butyl T_8	19.1	19.8	26.9
Fluorodecyl T_8	9.3	10.2	8.8
Fluorodecyl Q_4	14.3	20.1	14.9
Fluorodecyl M_2	26.8	--	39.7

*All liquids include a set of n-alkanes from pentane to hexadecane, rapeseed oil, dimethyl sulfoxide, ethylene glycol, diiodomethane, and water.

Assuming a typical error in contact angle measurement ($\Delta\theta \approx 2^\circ$), and from the condition number of the transformation matrix in the system of linear equations, a 15% relative error ($\delta\gamma_{sv}/\gamma_{sv}$) is expected in the computed values of the surface energies.

Table 3. Computed values of the dispersion (γ_{sv}^d), acidic (γ_{sv}^+), and basic (γ_{sv}^-) components of solid surface energy (mN/m) for various fluoroalkylated silicon containing moieties are summarized.

γ_{sv} (mN/m)	Alkanes (Zisman analysis)	All liquids* (Equation 1 with $\phi_{sl} = 1$)	Diiodomethane, dimethyl sulfoxide and water (Equation 5)				
	γ_c	γ_{sv}	γ_{sv}	Dispersion (γ_{sv}^d)	Polar (γ_{sv}^p)	Acidic (γ_{sv}^+)	Basic (γ_{sv}^-)
Fluorodecyl T_8	5.5	9.3	8.8	8.7	0.1	0.04	0.1
Fluorooctyl T_8	7.4	10.6	10.9	10.6	0.3	0.2	0.1
Fluorohexyl T_8	8.5	11.6	47.4	11.4	36.0	20.8	15.6
Fluoropropyl T_8	19.7	18.7	38.4	19.1	19.3	11.8	7.9
Hexafluoro-<i>i</i>- butyl T_8	17.7	19.1	26.9	26.8	0.1	0.002	0.8
Fluorodecyl T_8	5.5	9.3	8.8	8.7	0.1	0.04	0.1
Fluorodecyl Q_4	14.5	14.3	14.9	14.5	0.8	0.0	0.2
Fluorodecyl M_2	19.6	26.8	39.7	30.9	8.8	2.0	9.7

The dispersion component of the solid surface energy (calculated in Table 3) increased monotonically from fluorodecyl T_8 ($\gamma_{sv}^d = 8.7$ mN/m) to hexafluoro-*i*-butyl T_8 ($\gamma_{sv}^d = 26.8$ mN/m), whereas the polar component (γ_{sv}^p) does not follow any clear trend. The fluoroalkylated T_8 molecules have two methylene groups [one methylene and one methyne group in case of hexafluoro-*i*-butyl T_8] connecting the –Si–O– cage with the fluoroalkyl chain (see structure in Table 1). Methylene groups are non-polar, but due to the higher polarizability of a –CH₂– moiety (as compared with a –CF₂– moiety), the dispersion component of the solid surface energy tends to be higher (γ_{sv}^d for polyethylene $\approx 30 - 32$ mN/m, versus $\gamma_{sv}^d = 18 - 20$ mN/m for PTFE and 6.7 mN/m for a monolayer of –CF₃ groups). Therefore, this increase in γ_{sv}^d of the T_8 molecules is attributed to higher interaction of the contacting liquids with the underlying

$-\text{CH}_2-\text{CH}_2-$ and $(-\text{CF}_2)_n$ groups. As the length of the perfluorinated chain decreases, the crystalline-like packing of the side chains becomes unfavorable and the underlying $-\text{CF}_2-$ and $-\text{CH}_2-$ groups start contributing to the total solid surface energy.

Similarly, when we compare the fluorodecyl T_8 , Q_4 and M_2 molecules, we find that γ_{sv}^d increases monotonically from a T_8 cage (8.7 mN/m) to a Q_4 ring (14.5 mN/m) and finally to a M_2 straight chain (30.9 mN/m) and this increase in the dispersion component of the solid surface energy accounts for most of the increase in the total surface energy (γ_{sv}). The T_8 cage structure seems to achieve an optimal packing of the eight fluorodecyl chains, which results in very restricted ability to rearrange these chains when in contact with probing liquids. As a consequence, the fluorodecyl T_8 cage has the lowest solid surface energy among all the molecules tested. The behavior of T_8 surfaces with fluorinated chains longer than the fluorodecyl group (*i.e.* greater in length than $-(\text{CF}_2)_7\text{CF}_3$) is still an open question. Currently fluorododecyl and fluorotetradecyl T_8 synthesis is underway and the systematic analysis of their wettability will be the scope of a future investigation.

The main objective of this paper was to estimate the solid surface energy of the native solid surface. The discussion above is based on calculations of the solid surface energy obtained by substituting the advancing contact angle (θ_{adv}) in place of the equilibrium contact angle (θ_E) in the governing equations. The advancing contact angle (θ_{adv}) is the local value of the contact angle formed by a liquid droplet when it touches the solid surface for the first time, so the advancing contact angle (θ_{adv}) is the physically more relevant measurement to use rather than the receding contact angle (θ_{rec}) in the context of determining solid surface energies. Although uncontrolled local chemical inhomogeneities and dust contamination can contribute to contact angle hysteresis, we believe that the most important factor in the carefully controlled spin-coated flat surfaces studied in the present work is reorganization or reconstruction of the solid surface as a result of contact with the probing liquid. As a result, a finite contact angle hysteresis ($\Delta\theta = \theta_{adv} - \theta_{rec}$) was observed for all the molecules studied here. Substituting the advancing contact angles (θ_{adv}) on a flat surface in place of the equilibrium contact angle (θ_E), into

the Girifalco-Good equation leads to a value of solid surface energy (say $\gamma_{sv,a}$), while substituting receding contact angles (θ_{rec}), yields a higher value of solid surface energy (say $\gamma_{sv,r} > \gamma_{sv,a}$) *i.e.*

$$\cos \theta_{adv} = -1 + 2\phi_{sl} \sqrt{\frac{\gamma_{sv,a}}{\gamma_{lv}}} \quad \text{and} \quad \cos \theta_{rec} = -1 + 2\phi_{sl} \sqrt{\frac{\gamma_{sv,r}}{\gamma_{lv}}}. \quad \text{If the difference between } \gamma_{sv,r} \text{ and } \gamma_{sv,a} \text{ is small, a}$$

low energy solid surface has the desirable attribute of being able to resist reorganization in the presence of the contacting liquid. As shown in Table S6 of the supporting information, fluorodecyl T_8 exhibits lowest value of $\gamma_{sv,r} - \gamma_{sv,a}$ (≈ 7 mN/m). Fluorodecyl Q_4 and fluorodecyl M_2 molecules are more susceptible to rearrangements in contact with probing liquids, as indicated by comparatively higher values of $\gamma_{sv,r} - \gamma_{sv,a}$, 12.2 and 9.0 mN/m respectively. In the case of molecules with a T_8 cage, the fluoropropyl molecule has equally low value of $\gamma_{sv,r} - \gamma_{sv,a}$ as that measured for fluorodecyl T_8 , though the inherent solid surface energy is much higher for the fluoropropyl T_8 molecule ($\gamma_{sv} = 18.7$ vs. 9.3 mN/m for fluorodecyl T_8). (See supporting information Table S6 for more details on the analysis of contact angle hysteresis ($\gamma_{sv,r} - \gamma_{sv,a}$) on various solid surfaces.)

Thus, we note that the special character of fluorodecyl POSS (lowest solid surface energy $\gamma_{sv} = 9.3$ mN/m along with maximum resistance to solid surface reconstruction and thus low contact angle hysteresis) apparently arises from the favorable combination of the cage structure and the fluorodecyl side chains. The latter contribute to an unusually low value of dispersive contribution to the solid surface energy while simultaneously reducing polar contributions to nearly zero. The cage structure is relatively inflexible towards molecular reorganization compared to the ring or linear analogs. Whether or not fluorodecyl side chain represents the optimal substituent remains an open question. A plot of solid surface energy (γ_{sv}) versus cage substituent chain length (Figure S4 in the supporting information) suggests that a minimum may not yet have been achieved with the fluorodecyl substituent. Synthesis of the dodecyl and tetradecyl analogs is now underway to explore this unanswered question. We note, however, that very long fluoroalkyl chains on the POSS cage should eventually produce PTFE-like surface energies in the range of $\gamma_{sv} = 18$ -20 mN/m, well above the value of $\gamma_{sv} = 9.3$ mN/m found here for the fluorodecyl cage molecule.

Conclusions

The solid surface energy (γ_{sv}) plays a key role in controlling the equilibrium contact angle (θ_E) and subsequently the robustness (P_b) of a liquid droplet and apparent contact angle (θ^*) on a textured surface that enables a solid-liquid-air composite interface to be established. Smooth fluorodecyl POSS surfaces lead to one of the highest known equilibrium contact angles (θ_E) at the 3-phase contact line. To investigate why fluorodecyl POSS performs so well as a non-wetting coating, a series of fluoroalkylated silicon-containing molecules resembling fluorodecyl POSS were synthesized. Their wettability characteristics were assessed using (1) Zisman analysis with a set of n-alkanes and (2) Girifalco-Good analysis using a broad range of polar and non-polar liquids. Both the critical surface tension (γ_c) and the calculated value of solid surface energy (γ_{sv}) follow the same trend: The solid surface energy increased monotonically from $\gamma_{sv} = 9.3$ to $\gamma_{sv} = 18.7$ mN/m as the length of the perfluorinated chain was reduced from fluorodecyl to fluoropropyl T_8 POSS and as the dimensionality of the cage was reduced from 9.3 mN/m for fluorodecyl T_8 3D cage to 14.3 mN/m for fluorodecyl Q_4 ring and 26.8 mN/m for a fluorodecyl M_2 linear chain molecule. Hydrogen bond donating (γ^+), hydrogen bond accepting (γ^{\ominus}), polar (γ^p) and dispersion components (γ^d) of the total solid surface energy were also individually computed using two sets of probing liquids (dodecane, acetone, chloroform and water, diiodomethane, dimethyl sulfoxide respectively). Of the fluorinated molecules tested so far, fluorodecyl T_8 has the lowest solid surface energy ($\gamma_{sv} = 9.3$ mN/m) along with the lowest degree of surface reorganization, manifested through a lowest increment in the solid surface energy ($\Delta\gamma_{sv} = 7.0$ mN/m) in contact with probing liquids. This desirable property arises probably due to the synergy between a rigid T_8 cage surrounded by long fluorodecyl side chains.

ACKNOWLEDGMENT

This research was supported by the Army Research Office (ARO) through contract no. W911NF-07-D-0004. Financial support was also provided by the Air Force Office of Scientific Research and the Air Force Research laboratory, Propulsion Directorate. We thank Prof. Michael Rubner and the Institute of Soldier Nanotechnologies (ISN) at MIT for the use of various experimental facilities, Ms. Wui Siew Tan and Mr. Siddharth Srinivasan for help with the AFM characterization, and Dr. Adam J. Meuler for helpful discussion during the preparation of this manuscript.

Supporting Information Available.

The supporting information includes raw contact angle data, quantification about the deviation of the contact angle data from the Zisman line and the Girifalco-Good curve, liquid surface tension values used for solid surface energy calculations, and computed values of the solid surface energy. This material is available free of charge via the Internet at <http://pubs.acs.org>.

REFERENCES

1. Lafuma, A.; Quéré, D. *Nat Mater* **2003**, 2, 457-460.
2. Ma, M.; Hill, R. M.; Rutledge, G. C. *J. Adhes. Sci. Technol.* **2008**, 22, 1799-1817.
3. Ma, M.; Mao, Y.; Gupta, M.; Gleason, K. K.; Rutledge, G. C. *Macromolecules* **2005**, 38, 9742-9748.
4. Michielsen, S.; Lee, H. J. *Langmuir* **2007**, 23, 6004-6010.
5. Ahuja, A.; Taylor, J. A.; Lifton, V.; Sidorenko, A. A.; Salamon, T. R.; Lobaton, E. J.; Kolodner, P.; Krupenkin, T. N. *Langmuir* **2008**, 24, 9-14.
6. Brewer, S. A.; Willis, C. R. *Appl. Surf. Sci.* **2008**, 254, 6450-6454.
7. Chhatre, S. S.; Choi, W.; Tuteja, A.; Park, K.-C.; Mabry, J. M.; McKinley, G. H.; Cohen, R. E. *Langmuir* **2010**, 26, 4027-4035.
8. Chhatre, S. S.; Tuteja, A.; Choi, W.; Revaux, A. I.; Smith, D.; Mabry, J. M.; McKinley, G. H.; Cohen, R. E. *Langmuir* **2009**, 25, 13625-13632.
9. Choi, W.; Tuteja, A.; Chhatre, S.; Mabry, J. M.; Cohen, R. E.; McKinley, G. H. *Adv. Mat.* **2009**, 21, 2190-2195.
10. Choi, W.; Tuteja, A.; Mabry, J. M.; Cohen, R. E.; McKinley, G. H. *J. Colloid Interface Sci.* **2009**, 339, 208-216.
11. Tuteja, A.; Choi, W.; Ma, M.; Mabry, J. M.; Mazzella, S. A.; Rutledge, G. C.; McKinley, G. H.; Cohen, R. E. *Science* **2007**, 318, 1618-1622.
12. Tuteja, A.; Choi, W.; Mabry, J. M.; McKinley, G. H.; Cohen, R. E. *Proc. Natl. Acad. Sci. USA* **2008**, 18200-18205.
13. Tuteja, A.; Choi, W.; McKinley, G. H.; Cohen, R. E.; Rubner, M. F. *MRS Bull.* **2008**, 33, 752-758.
14. Hoefnagels, H. F.; Wu, D.; deWith, G.; Ming, W. *Langmuir* **2007**, 23, 13158-13163.
15. Leng, B.; Shao, Z.; de With, G.; Ming, W. *Langmuir* **2009**, 25, 2456-2460.
16. Marmur, A. *Langmuir* **2008**, 24, 7573-7579.
17. Cassie, A.; Baxter, S. T. *Faraday Soc.* **1944**, 40, 546-551.
18. Mabry, J.; Vij, A.; Iacono, S.; Viers, B. *Angew. Chem. Int. Ed.* **2008**, 47, 4137-4140.
19. Zisman, W. A., *Relation of the equilibrium contact angle to liquid and solid construction.* American Chemical Society, Washington DC: 1964.
20. Owens, D. K.; Wendt, R. C. *J. Appl. Polym. Sci.* **1969**, 13, 1741-1747.
21. Good, R. J. *J. Colloid Interface Sci.* **1977**, 59, 398-419.
22. Good, R. J. *J. Adhes. Sci. Technol.* **1992**, 6, 1269-1302.
23. Iacono, S. T.; Vij, A.; Grabow, W.; Smith, D. W.; Jr; Mabry, J. M. *Chem. Commun.* **2007**, 4992-4994.
24. Goodwin, G. B.; Kenney, M. E. Novel Route to Ca₈Si₄O₁₂Cl₈ Alkosycyclotetrasiloxanes, Aryloxycyclotetrasiloxanes, Alkylcyclotetrasiloxanes and Arylcyclotetrasiloxanes from Wollastonite (CaSiO₃). 4824985, 1989.
25. Teng, C. J.; Cai, G.; Weber, W. P. *J. Fluorine Chem.* **2004**, 125, 1451-1455.
26. Lentz, C. W. *Inorg. Chem.* **1964**, 3, 574-579.
27. Bennett, M. K.; Zisman, W. A. *J. Phys. Chem.* **1960**, 64, 1292-1294.
28. Bennett, M. K.; Zisman, W. A. *J. Phys. Chem.* **1973**, 77, 2324-2328.
29. Ellison, A. H.; Fox, H. W.; Zisman, W. A. *J. Phys. Chem.* **1953**, 57, 622-627.
30. Ellison, A. H.; Zisman, W. A. *J. Phys. Chem.* **1954**, 58, 503-506.
31. Ellison, A. H.; Zisman, W. A. *J. Phys. Chem.* **1954**, 58, 260-265.
32. Fox, H. W.; Hare, E. F.; Zisman, W. A. *J. Coll. Sci.* **1953**, 8, 194-203.
33. Schulman, F.; Zisman, W. A. *J. Coll. Sci.* **1952**, 7, 465-481.
34. Shafrin, E. G.; Zisman, W. A. *J. Phys. Chem.* **1962**, 66, 740-748.
35. Bennett, M. K.; Zisman, W. A. *J. Phys. Chem.* **1962**, 66, 1207-1208.

36. Fox, H. W.; Zisman, W. A. *J. Coll. Sci.* **1950**, 5, 514-531.
37. Fox, H. W.; Zisman, W. A. *J. Coll. Sci.* **1952**, 7, 109-121.
38. Fox, H. W.; Zisman, W. A. *J. Coll. Sci.* **1952**, 7, 428-442.
39. Chaudhury, M. K. *Mat. Sci. Eng. R.* **1996**, 16, 97-159.
40. Girifalco, L. A.; Good, R. J. *J. Phys. Chem.* **1957**, 61, 904-909.
41. Good, R. J.; Girifalco, L. A. *J. Phys. Chem.* **1960**, 64, 561-565.
42. Van Oss, C. J.; Chaudhury, M. K.; Good, R. J. *Chem. Rev.* **1988**, 88, 927-941.
43. Van Oss, C. J.; Good, R. J.; Chaudhury, M. K. *Langmuir* **1988**, 4, 884-891.
44. Johnson, R. E.; Dettre, R. H., *Wetting of Low-Energy surfaces*. Marcel Dekker: New York, 1993; p 1-74.
45. Nishino, T.; Meguro, M.; Nakamae, K.; Matsushita, M.; Ueda, Y. *Langmuir* **1999**, 15, 4321-4323.
46. Volpe, C. D.; Siboni, S. *J. Colloid Interface Sci.* **1997**, 195, 121-136.
47. Van Oss, C. J., *Interfacial Forces in Aqueous Media*. Marcel Dekker, Inc.: New York, 1994; p 18-45.
48. Shalel-Levanon, S.; Marmur, A. *J. Colloid Interface Sci.* **2003**, 262, 489-499.
49. Lemal, D. M. *J. Org. Chem.* **2004**, 69, 1-11.
50. O'Hagan, D. *Chem. Soc. Rev.* **2008**, 37, 308-319.

Fluoroalkylated Silicon-Containing Surfaces –

Estimation of Solid Surface Energy

Shreerang S. Chhatre,[†] Jesus O. Guardado,^{} Brian M. Moore,[§] Timothy S. Haddad,[‡] Joseph M. Mabry,*

[§] Gareth H. McKinley,^{‡} and Robert E. Cohen^{†*}*

Supporting Information Paragraph –

Table S1. Estimated values of solid surface energy (γ_{sv}) along with 95% confidence intervals are shown here.

Molecule	γ_{sv} (mN/m) (mean)	95% confidence interval (mN/m)		Standard deviation (σ) (mN/m)
Fluorodecyl T_8	9.3	4.5	14.1	2.4
Fluorooctyl T_8	10.6	5.7	15.4	2.4
Fluorohexyl T_8	11.6	6.7	16.3	2.4
Fluoropropyl T_8	18.7	13.9	23.5	2.4
Hexafluoro-i-butyl T_8	19.1	14.3	23.9	2.4
Fluorodecyl T_8	9.3	4.5	14.1	2.4
Fluorodecyl Q_4	14.3	9.5	19.1	2.4
Fluorodecyl M_2	26.8	18.2	27.9	2.4

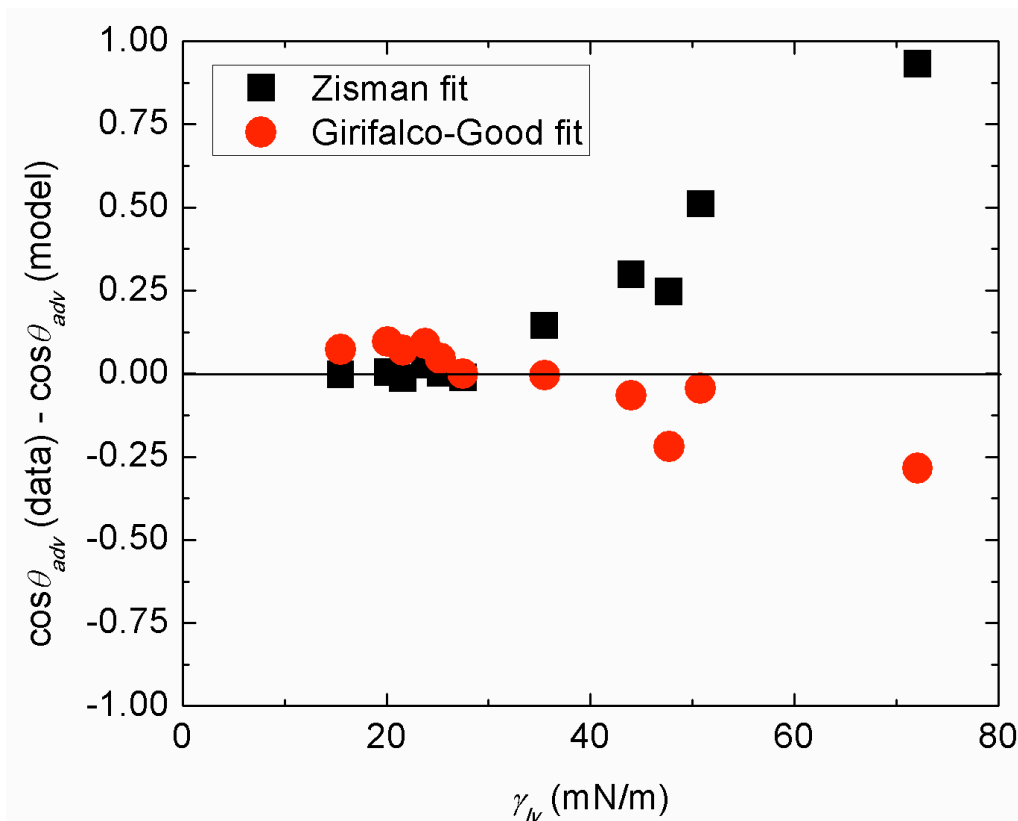


Figure S1. The difference (r) between measured value of the cosine of advancing contact angle ($\cos\theta_{adv}$) and the cosine of the expected contact angle from the Zisman as well as the Girifalco-Good relation is plotted against the liquid surface tension (γ_{lv}). The Girifalco-Good relation is a better fit to the data with a much smaller summation of the residual ($\sum r = -0.25$) compared to the Zisman analysis ($\sum r = 2.13$).

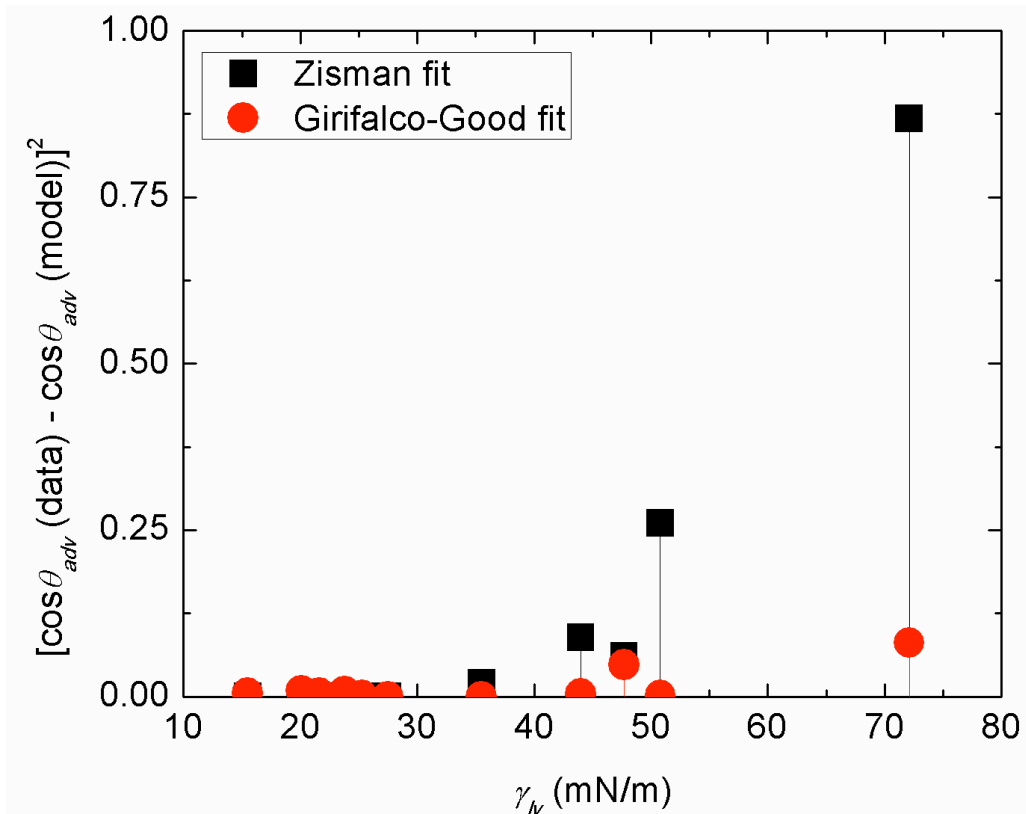


Figure S2. The square of the difference (r) between measured value of the cosine of advancing contact angle ($\cos\theta_{adv}$) and the cosine of the expected contact angle from the Zisman as well as the Girifalco-Good relation is plotted against the liquid surface tension (γ_{lv}). The Girifalco-Good relation is a better fit to the data with a much smaller summation of the squares of the residual ($\sum r^2 = 0.16$) compared to the Zisman analysis ($\sum r^2 = 1.30$).

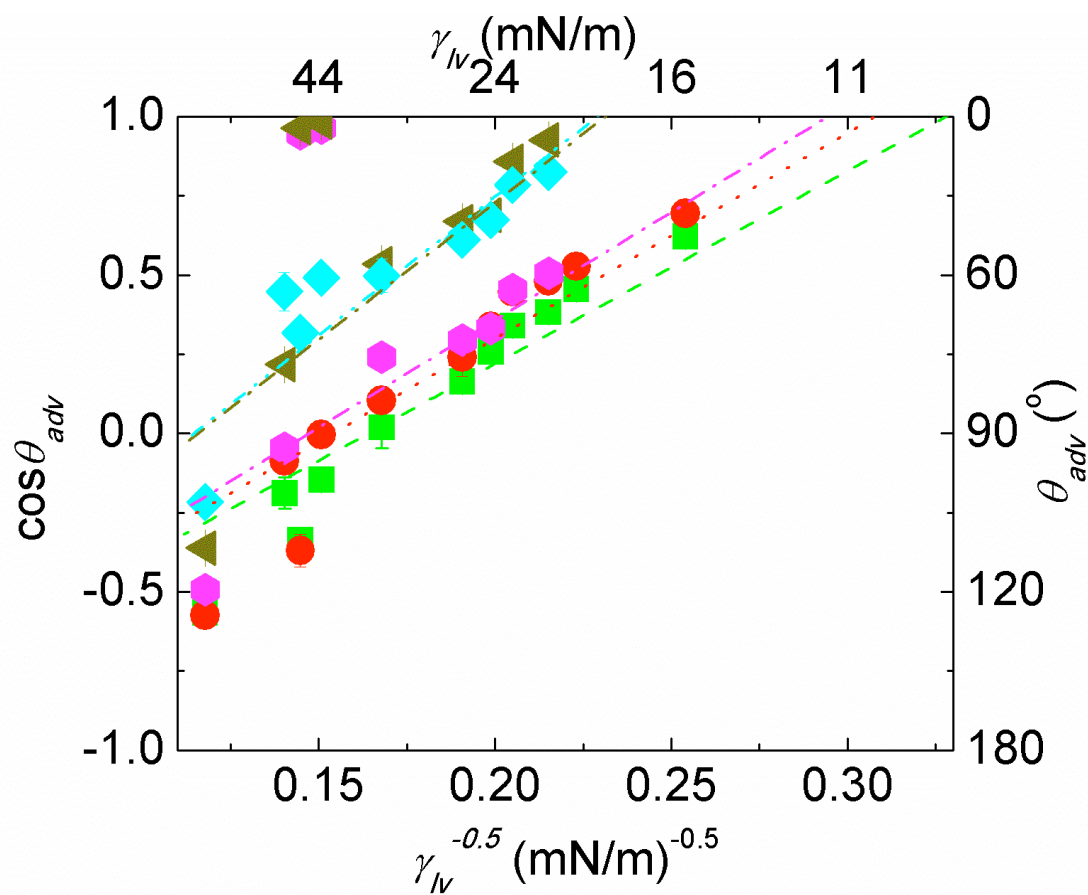


Figure S3. The data in Figure 3 (cosine of the advancing contact angle on various T_8 surfaces) are replotted against inverse square root of liquid surface tension. Best fit Girifalco-Good lines are plotted using Equation 1 with $\square_l = 1$.

Table S2. Computed values of solid surface energy (γ_{sv} mN/m) for various fluoroalkylated silicon containing moieties are summarized.

γ_{sv} (mN/m) based on contact angles ($^\circ$) of the probing liquids	All liquids* (Equation 1 with $\square_l = 1$)	Dodecane, acetone, and chloroform (Equation 5)	Diiodomethane, dimethyl sulfoxide and water (Equation 5)	All liquids* (Equation 1 with $\square_l = 1$)	Dodecane, acetone, and chloroform (Equation 5)	Diiodomethane, dimethyl sulfoxide and water (Equation 5)
	Advancing			Receding		
Fluorodecyl T_8	9.3	10.2	8.8	16.3	14.9	18.0
Fluorooctyl T_8	10.6	13.6	10.9	19.7	20.9	21.7
Fluorohexyl T_8	11.6	26.8	47.4	24.0	27.4	38.2
Fluoropropyl T_8	18.7	21.4	38.4	25.7	21.9	31.2
Hexafluoro-<i>i</i>-butyl T_8	19.1	19.8	26.9	28.5	21.6	42.5
Fluorodecyl T_8	9.3	10.2	8.8	16.5	14.9	18.0
Fluorodecyl Q_4	14.3	20.1	14.9	26.5	24.3	38.8
Fluorodecyl M_2	23.0	--	39.7	32.0	--	43.1

*All liquids include a set of n-alkanes from pentane to hexadecane, rapeseed oil, dimethyl sulfoxide, ethylene glycol, diiodomethane, and water.

Assuming a typical error in contact angle measurement ($\Delta\theta \approx 2^\circ$), and from the condition number of the transformation matrix in the system of linear equations, a 15% relative error ($\delta\gamma_{sv}/\gamma_{sv}$) is expected in the computed values of the surface energies.

Table S3. Values of hydrogen bond donating (γ_{lv}^+), hydrogen bond accepting (γ_{lv}^-), polar (γ_{lv}^p), dispersion (γ_{lv}^d), and total liquid surface tension (γ_{lv}) in mN/m used for the estimation of solid surface energy are summarized. [Taken from - Chaudhury, M. K. *Mat. Sci. Eng. R.* **1996**, 16, 97-159.]

Liquid	γ_{lv}	γ_{lv}^d	γ_{lv}^p	γ_{lv}^+	γ_{lv}^-
Acetone	25.2	25.2	0.0	0.0	24.0
Chloroform	27.5	27.5	0.0	3.8	0.0
Dimethyl sulfoxide	44.0	36.0	8.0	0.5	32
Water	72.1	21.1	51.0	25.5	25.5
Ethylene glycol	47.7	28.7	19.0	1.9	47.0
Diiodomethane	50.8	50.8	0.0	0.0	0.0
Rapeseed oil	35.5	35.5	0.0	0.0	0.0
Hexadecane	27.5	27.5	0.0	0.0	0.0
Dodecane	25.3	25.3	0.0	0.0	0.0
Decane	23.8	23.8	0.0	0.0	0.0
Octane	21.6	21.6	0.0	0.0	0.0
Heptane	20.1	20.1	0.0	0.0	0.0
Pentane	15.5	15.5	0.0	0.0	0.0

Table S4. Values of the advancing contact angles (θ_{adv}) for liquid droplets with a wide range of surface tensions on a flat silicon wafer spin-coated with fluoroalkylated silicon-containing compounds are summarized.

Solid liquid /	Fluorodecyl T_8	Fluorooctyl T_8	Fluorohexyl T_8	Fluoropropyl T_8	Hexafluoro- <i>i</i> -butyl T_8	Fluorodecyl M_8Q_4	Fluorodecyl M_2
Water	122 ± 2°	122 ± 2°	120 ± 1°	111 ± 1°	102 ± 2°	114 ± 2°	70 ± 2°
Diiodomethane	100 ± 2°	95 ± 1°	93 ± 1°	77 ± 2°	63 ± 4°	87 ± 3°	56 ± 4°
Ethylene glycol	111 ± 2°	112 ± 3°	19 ± 2°	15 ± 2°	71 ± 2°	94 ± 2°	56 ± 5°
Dimethyl sulfoxide	98 ± 2°	90 ± 2°	15 ± 2°	11 ± 2°	63 ± 2°	81 ± 2°	12 ± 3°
Rapeseed oil	88 ± 3°	84 ± 1°	76 ± 1°	58 ± 1°	60 ± 4°	69 ± 2°	39 ± 3°
Hexadecane	80 ± 1°	76 ± 4°	73 ± 1°	48 ± 2°	52 ± 2°	66 ± 2°	34 ± 2°
Dodecane	75 ± 1°	70 ± 1°	71 ± 2°	47 ± 1°	48 ± 2°	62 ± 2°	30 ± 4°
Decane	70 ± 2°	63 ± 1°	63 ± 1°	31 ± 1°	38 ± 2°	55 ± 1°	23 ± 1°
Octane	67 ± 1°	61 ± 2°	60 ± 1°	22 ± 3°	34 ± 2°	43 ± 2°	13 ± 1°
Heptane	63 ± 2°	58 ± 2°	54 ± 2°	17 ± 1°	25 ± 3°	32 ± 4°	13 ± 3°
Pentane	52 ± 1°	46 ± 2°	43 ± 2°	14 ± 1°	17 ± 1°	23 ± 1°	< 10°

Table S5. Values of the receding contact angles (θ_{rec}) for liquid droplets with a wide range of surface tensions on a flat silicon wafer spin-coated with fluoroalkylated silicon-containing compounds are summarized.

Solid liquid /	Fluorodecyl T_8	Fluorooctyl T_8	Fluorohexyl T_8	Fluoropropyl T_8	Hexafluoro- <i>i</i> -butyl T_8	Fluorodecyl M_8Q_4	Fluorodecyl M_2
Water	$116 \pm 2^\circ$	$97 \pm 2^\circ$	$103 \pm 4^\circ$	$95 \pm 2^\circ$	$61 \pm 2^\circ$	$74 \pm 3^\circ$	$45 \pm 3^\circ$
Diiodomethane	$79 \pm 3^\circ$	$76 \pm 3^\circ$	$77 \pm 1^\circ$	$59 \pm 2^\circ$	$40 \pm 2^\circ$	$55 \pm 2^\circ$	$41 \pm 1^\circ$
Ethylene glycol	$87 \pm 1^\circ$	$82 \pm 3^\circ$	$< 10^\circ$	$< 10^\circ$	$24 \pm 4^\circ$	$60 \pm 2^\circ$	$40 \pm 2^\circ$
Dimethyl sulfoxide	$80 \pm 5^\circ$	$78 \pm 2^\circ$	$< 10^\circ$	$< 10^\circ$	$19 \pm 2^\circ$	$61 \pm 7^\circ$	$< 10^\circ$
Rapeseed oil	$66 \pm 3^\circ$	$42 \pm 2^\circ$	$37 \pm 4^\circ$	$25 \pm 3^\circ$	$23 \pm 6^\circ$	$21 \pm 2^\circ$	$17 \pm 2^\circ$
Hexadecane	$61 \pm 3^\circ$	$45 \pm 2^\circ$	$39 \pm 2^\circ$	$39 \pm 3^\circ$	$37 \pm 3^\circ$	$20 \pm 1^\circ$	$18 \pm 2^\circ$
Dodecane	$60 \pm 4^\circ$	$35 \pm 2^\circ$	$36 \pm 4^\circ$	$34 \pm 2^\circ$	$40 \pm 2^\circ$	$17 \pm 2^\circ$	$14 \pm 2^\circ$
Decane	$44 \pm 2^\circ$	$30 \pm 2^\circ$	$30 \pm 2^\circ$	$25 \pm 2^\circ$	$26 \pm 2^\circ$	$14 \pm 2^\circ$	$< 10^\circ$
Octane	$24 \pm 2^\circ$	$24 \pm 2^\circ$	$23 \pm 3^\circ$	$16 \pm 1^\circ$	$23 \pm 2^\circ$	$< 10^\circ$	$< 10^\circ$
Heptane	$19 \pm 4^\circ$	$14 \pm 1^\circ$	$15 \pm 3^\circ$	$12 \pm 2^\circ$	$18 \pm 2^\circ$	$< 10^\circ$	$< 10^\circ$
Pentane	$< 10^\circ$	$< 10^\circ$	$< 10^\circ$	$< 10^\circ$	$< 10^\circ$	$< 10^\circ$	$< 10^\circ$

Table S6. Computed values of solid surface energy (γ_{sv} mN/m) based on advancing and receding contact angles for various fluoroalkylated silicon containing moieties are summarized. From these values, various notions of contact angle hysteresis are computed.

γ_{sv} (mN/m) based on contact angles ($^\circ$) of the probing liquids	All liquids* (Equation 1 with $\square_l = 1$), based on –		$\gamma_{sv,r} - \gamma_{sv,a}$ mN/m	$\gamma_{sv,r}^{0.5} - \gamma_{sv,a}^{0.5}$ (mN/m) ^{0.5}	$\Delta = 2(1 - (\gamma_{sv,a} / \gamma_{sv,r})^{0.5})$
	advancing contact angles ($\gamma_{sv,a}$)	receding contact angles ($\gamma_{sv,r}$)			
Fluorodecyl T_8	9.3	16.3	7.0	0.99	0.49
Fluorooctyl T_8	10.6	19.7	9.2	1.19	0.54
Fluorohexyl T_8	11.6	24.0	12.5	1.51	0.61
Fluoropropyl T_8	18.7	25.7	7.0	0.74	0.29
Hexafluoro-i-butyl T_8	19.1	28.5	9.4	0.97	0.36
Fluorodecyl T_8	9.3	16.5	7.0	0.99	0.49
Fluorodecyl Q_4	14.3	26.5	12.2	1.36	0.53
Fluorodecyl M_2	23.0	32.0	9.0	0.86	0.30

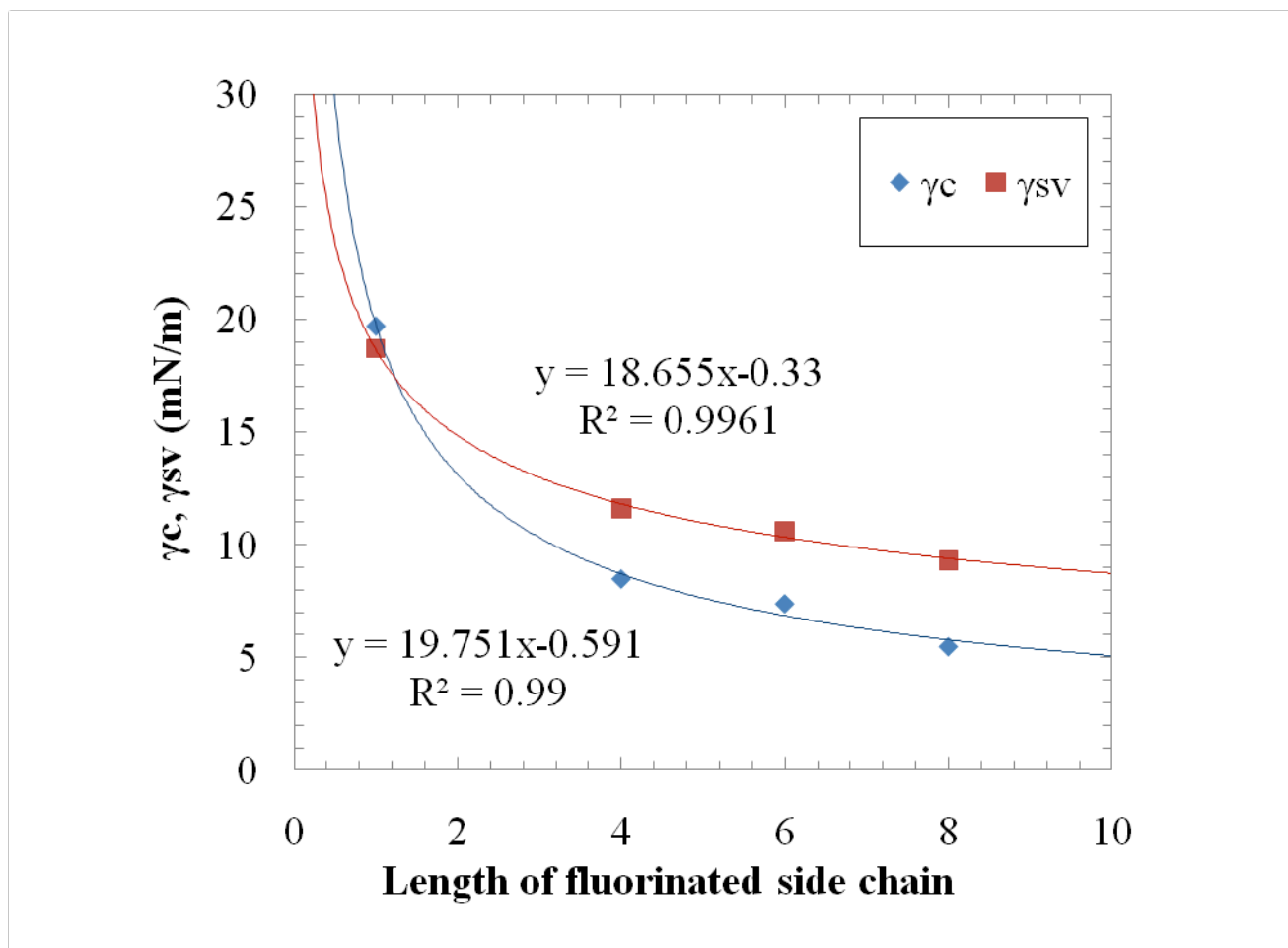
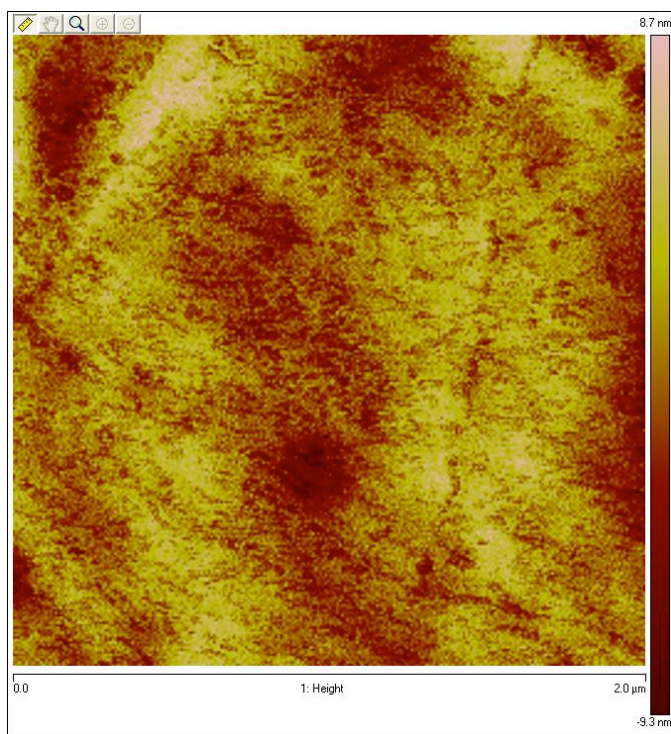


Figure S4. Solid surface energy (γ_{sv}) obtained by Girifalco-Good analysis and critical surface tension (γ_c) obtained by Zisman analysis is plotted against the length of fluorinated side chain for fluoroalylated T_8 molecules.

Table S7. Spin-coated silicon wafer samples were probed using tapping mode AFM to quantify roughness of these samples. Mean roughness (R_a) and root mean squared roughness (R_q) data is summarized in the following table. The Wenzel roughness (r) was computed by dividing the actual area recorded by the AFM by the projected area.

Solid surface	Roughness (nm)		Wenzel roughness (r)
	(rms, R_q)	(average, R_a)	
Fluorodecyl T_8	9.3	7.3	1.01
Fluorohexyl T_8	2.6	2.1	1.005
Fluoropropyl T_8	14.4	11.6	1.01
Hexafluoro-<i>i</i>-butyl T_8	18.4	13.8	1.01

(a)



(b)

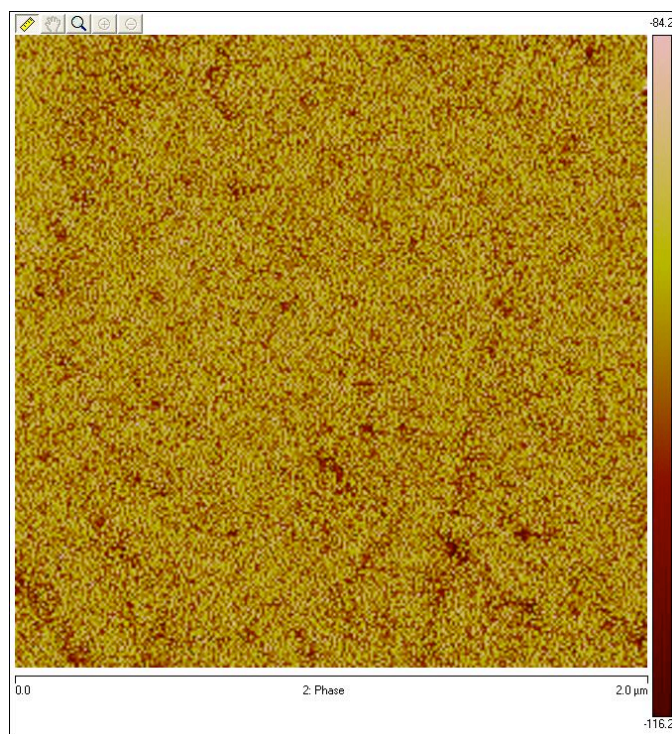


Figure S5. (a) Height and (b) phase images of AFM micrographs of a flat silicon wafer spin-coated with fluorohexyl T_8 is shown. The scale bar in (a) indicates height in nm and (b) indicates phase angle in degrees.